[American Journal of Science, Vol. 316, February, 2016, P. 169–201, DOI 10.2475/02.2016.03]

# RAPID FLUID FLOW ALONG FRACTURES AT GREENSCHIST FACIES CONDITIONS ON SYROS, GREECE

BARBARA I. KLEINE*,**,†, ZHIHONG ZHAO***, and ALASDAIR D.L. SKELTON**

**ABSTRACT. Brittle fractures cut through greenschist facies metavolcanic rocks at Delfini on Syros, Greece. An equation for one-dimensional transport by advection along a single fracture and transverse diffusion outwards from this fracture was used to calculate time-averaged fluid velocities and the duration of fluid flow along the brittle fractures. These quartz and carbonate filled fractures are surrounded by symmetrical dark reaction halos. These reaction halos were formed by diffusion of $CO_2$ outwards from the fracture in a hydrous fluid which caused carbonation of the country rock. Changes in concentration of relatively mobile elements (for example K, Na, Cs, Ba, Pb and Sr) occurred. However, little to no changes in most of the major elements and less mobile trace elements were observed. This implies that carbonation was largely isochemical with respect to most non-volatile components. The Sr/Ca ratio was used to model time-averaged fluid velocities and the duration of fluid flow along the fractures. Fluid flow along narrower fractures with discernibly tapering haloes was found to be rapid ($10^{-6}$ – $10^{-5}$ $ms^{-1}$) and short lived (0.1–400 years). These are time-averaged values and can therefore alternatively record a series of even shorter and faster pulses, perhaps associated with fracture propagation and associated seismicity. Within the widest fractures with constant halo widths (*ca.* 60 cm) fluid flow was slower ($10^{-8}$ to $10^{-6}$ $ms^{-1}$) and longer lived (100–15000 years). We suspect that the constant width of these haloes reflects a steady state having been reached at which halo width was controlled by the relative rates of fluid flow along the fracture and in the surrounding rock.**

Keywords: Fluid flow velocities, one-dimensional transport modeling, metamorphic fluid flow, carbonation, greenschist facies metamorphism

## INTRODUCTION

Metamorphic fluid-rock reactions preserve a record of the flux of volatiles and dissolved elements during orogenesis and provide in this way a basis for the quantification of time-integrated and time-averaged metamorphic fluid fluxes. Numerous studies throughout the last decades tackled the problem of calculating fluid flux rates from geological data. For example, estimations of 1-D time-integrated fluid fluxes were based on modeling the propagation of stable isotope fronts (Bickle and Baker, 1990) and reaction progress (Ferry, 1988; Baumgartner and Ferry, 1991) often at a high angle (approaching 90 degrees) to the fluid flow direction. These models were developed further to consider 2- or 3-D time-integrated fluid fluxes, for example by assuming or calculating that fluid flow was along a temperature gradient (Ague, 2007; Penniston-Dorland and Ferry, 2008), along thrust planes (McCaig and others, 1995; Abart and others, 2002) or along fold hinges (Skelton and others, 1995). Time-integrated fluxes of regional pervasive fluid flow range from 10 to $10^4$ $m^3m^{-2}$ during Barrovian metamorphism in New England and regional metamorphism in Scotland (Ferry, 1992; Léger and Ferry, 1993; Skelton and others, 1995; Evans and Bickle, 1999; Ague, 2003a). In the case of channelized fluid flow for example by shear zones, fold hinges, lithological layers or fractures, time-integrated fluid fluxes can become several orders of magnitude larger than fluxes of regional pervasive fluid flow (Ferry and

* Institute of Earth Science, University of Iceland, 101 Reykjavik, Iceland
** Department of Geological Sciences, Stockholm University, 106 91 Stockholm, Sweden, alasdair.skelton@geo.su.se
*** Department of Civil Engineering, Tsinghua University, Beijing, China, zhzhao@tsinghua.edu.cn
† Corresponding author: barbarak@hi.is, Tel: + 46 (0)8 16 4750, Fax: +46 (0) 8 674 78 97

Dipple, 1991; Ague, 1994a, 1994b, 1997, 2003b, 2011; Skelton and others, 1995; Breeding and Ague, 2002; Penniston-Dorland and Ferry, 2008; Miller and others, 2009; Kleine and others, 2014; Pogge von Strandmann and others, 2015). These large fluxes are able to cause significant mass transfer of rock-forming elements (Penniston-Dorland and Ferry, 2008; Miller and others, 2009; Beinlich and others, 2010; Ague, 2011; Herms and others, 2012; Pogge von Strandmann and others, 2015) and might even be large enough to transport heat (Ferry, 1992; Ague, 1994b; Camacho and others, 2005).

While time-integrated fluid fluxes give information about the total volume of fluid that has passed through a unit area of rock throughout an entire metamorphic event, time-averaged fluid fluxes provide some constraints about the rate and duration of metamorphic fluid flow (Walther and Orville, 1982; Brady, 1988; Connolly and Thompson, 1989; Peacock, 1989; Camacho and others, 2005; Skelton, 2011; John and others, 2012; Zhao and Skelton, 2013). Calculations of time-averaged fluid fluxes are always compared with a process for which the rate is known. This can be, for example experimentally determined diffusion rates (Wark and Watson, 2004). Time-averaged fluid fluxes have been calculated in 2- or 3-D from, for example, measurements of coupled advective displacement and diffusive broadening of geochemical fronts by assuming that fluid flow was along a fold hinge (Skelton, 2011; Zhao and Skelton, 2013). In these studies it was shown that metamorphic fluid flow events are relatively short-lived occurring on timescales of less than $10^4$ years and that fluid fluxes are $10^{-10.2\pm0.4}$ $m^3m^2s^{-1}$. This is in agreement with the findings of Camacho and others (2005) who calculated the time-integrated duration of an orogenic cycle on 13 Myr and the associated metamorphic events to be ~20 kyr. Even shorter time periods were reported by John and others (2012) who showed using Li-diffusion modeling that fluids released by dehydration in subducting slabs are mobilized in a series of short pulses lasting only 200 years. Recently, Kleine and others (2014) calculated that the fluid flux along a shear zone, also on Syros, was 100 to 2000 times faster than within surrounding rocks.

In this study we take advantage of a spectacular outcrop near the village of Delfini which is on the west side of Syros Island in the Greek Cyclades. Here, conjugate fractures in quartz-mica schists are filled with carbonates and quartz and rimmed by conspicuous symmetric reaction haloes. The haloes taper discernibly upwards, making it possible to calculate time-averaged fluid fluxes in a scenario where the direction of fluid flow is known (at least in 2-D), that is along the fractures. Because porosity within the fracture is likely to be large (≈1), we refer to fluid velocities rather than fluid fluxes in this paper.

## GEOLOGICAL BACKGROUND

The study area is located on the west side of the island Syros which belongs to the Cycladic archipelago in the Aegean Sea, Greece (fig. 1). Syros is now located in the back-arc of the active Hellenic subduction zone (Aubouin and Dercourt, 1965; Dürr and others, 1978; Jacobshagen and others, 1978; Jolivet and Brun, 2010). Most of the rocks on Syros belong to a subunit of the Attic-Cycladic core complex, known as the Cycladic Blueschist Unit (CBU) with a pre-Alpine basement followed by a sequence of metamorphosed volcano-sedimentary rocks (Dürr and others, 1978; Okrusch and Bröcker, 1990). Peak metamorphism occurred in the eclogite facies at 1.5 to 1.9 GPa and 500 to 525 °C (Trotet and others, 2001a; Trotet and others, 2001b; Schumacher and others, 2008a) and has been dated at 52 Ma (Maluski and others, 1987; Trotet and others, 2001b; Tomaschek and others, 2003; Putlitz and others, 2005; Cosca and Schumacher, 2005; Lagos and others, 2007). On Syros, greenschist facies retrogression occurred at 0.9 to 0.4 GPa and 500 to 350 °C (Avigad and others, 1992; Bröcker and others, 1993; Trotet and others, 2001b; Parra and others, 2002; Schumacher and

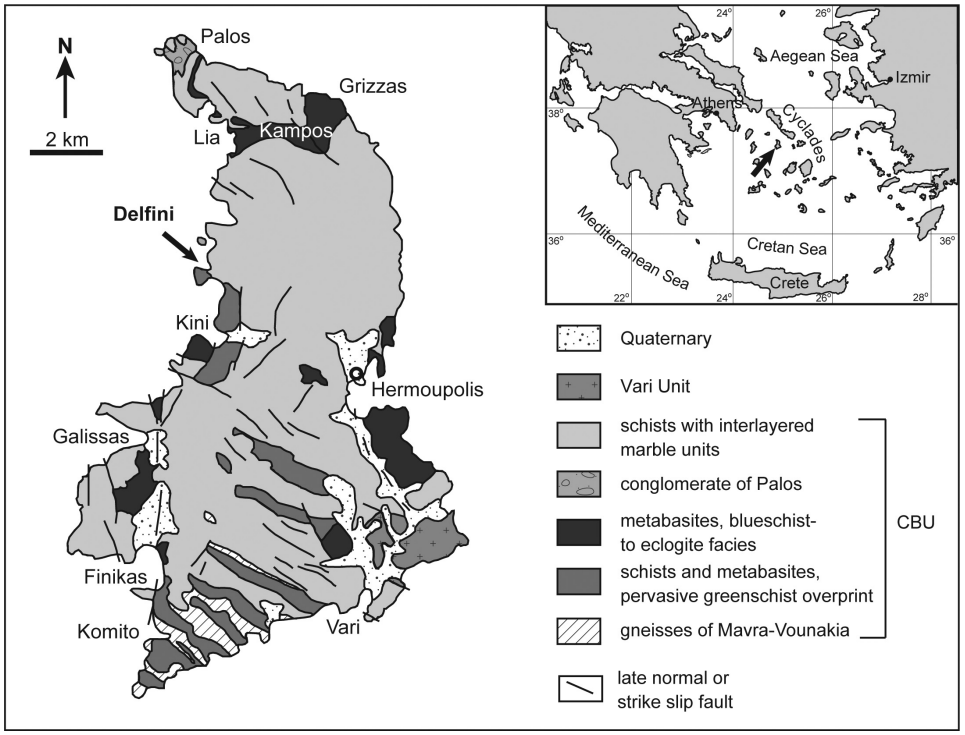


Fig. 1. Simplified geological map of Syros (modified after Keiter and others, 2011). The arrow indicates the studied area at Delfini.

others, 2008a) during Miocene times (Altherr and others, 1979; Wijbrans and others, 1990; Avigad, 1993; Bröcker and others, 1993; Bröcker and others, 2004).

## METAMORPHIC FLUID FLOW IN THE CYCLADES

Metamorphic rocks on Syros have been affected by fluid flow during prograde and retrograde metamorphism. These rocks have also been affected by late stage fracture-controlled fluid flow.

During prograde blueschist to eclogite facies metamorphism of subducting oceanic rocks, metamorphic fluids were strongly channeled (Bröcker and others, 1993; Ganor and others, 1996; Putlitz and others, 2000; Breeding and others, 2003; Ague, 2007) preferentially leaching LILEs, U, B and Pb as they passed through subducting metasedimentary rocks (Breeding and others, 2004; Marschall and others, 2006). Fluid generation in the subduction zone was likely to occur in relatively short-lived pulses (Pogge von Strandmann and others, 2015). Mixing and redistribution of major and trace elements led to the formation of hybrid rocks in the mélange zone (Miller and others, 2009). HP-rocks within the mélange zone are rimmed by so-called blackwalls that formed at a depth of 20 to 25 km at temperatures of 400 to 300 °C by the infiltration of a hydrous fluid derived from the subducting slab (Marschall and others, 2006). Kleine and others (2014) found evidence that HP-LT rocks underwent locally pervasive carbonation during or after peak metamorphism.

Retrogression at greenschist facies conditions was accompanied by pervasive flow of $^{18}O$-enriched metamorphic fluids (Schliestedt and Matthews, 1987) which caused hydration and decarbonation reactions in the HP-LT rocks (Kleine and others, 2014).

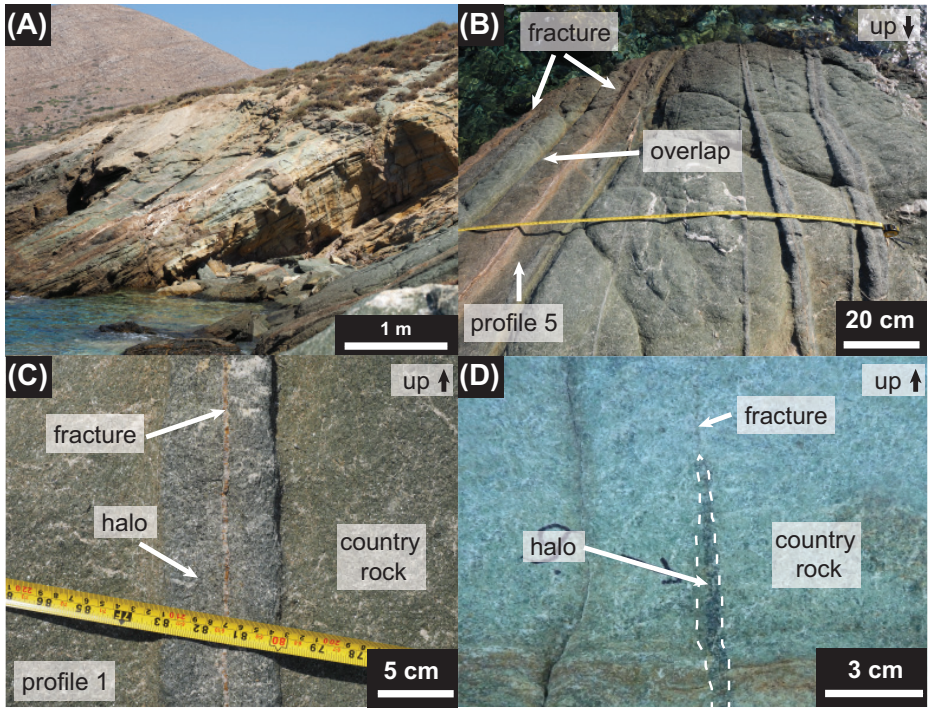


Fig. 2. (A) Field photography of the studied locality. (B) Field photography showing the five fracture-halo systems that were used for petrographic and geochemical analyses. There is a likely overlap of two halos from two different fractures in profile 5. (C) Close-up field photography of a fracture with a surrounding dark halo of profile 1. (D) Upwards tapering of the halo along a fracture at Delfini.

Both prograde and retrograde metamorphic fluids on Syros have been hydrous (Schumacher and others, 2008b) and variably saline (Barr, 1990).

Swarms of late stage carbonate and quartz veins cross cut variably preserved and retrograded high P – low T metamorphic rocks on Sifnos, Tinos and Kythnos (Ganor and others, 1994). These fluids were characterized by low $\delta^{13}C$ values (−12 ‰ to −8 ‰) due to oxidation of organic carbon or circulation of surface water through extensional fractures generated during late stage exhumation (Ganor and others, 1994; Famin and others, 2004).

At the west side of Syros a network of cross cutting quartz-carbonate filled fractures provides evidence of late stage fluid flow (fig. 2). These fractures have spectacular reaction halos which we use in this study to model late stage fluid flow on Syros.

## STUDY AREA

The studied outcrop is located along the northern shoreline of a small peninsula north of the village Delfini, on the western side of Syros (latitude: 37°27'40"N, longitude: 24°53'35"E). The rocks belong to a metamorphosed volcano-sedimentary subunit of the CBU and consist of quartz-mica schists with some preserved blueschist facies minerals which were partly and in some places completely overprinted at greenschist facies conditions. The outcrop hosts steeply dipping conjugate fractures which are filled by 0.2 to 2 cm wide carbonate-quartz filled fractures. The average orientations of the conjugate fracture sets are 248/77 and 168/74 (fig. 3) which

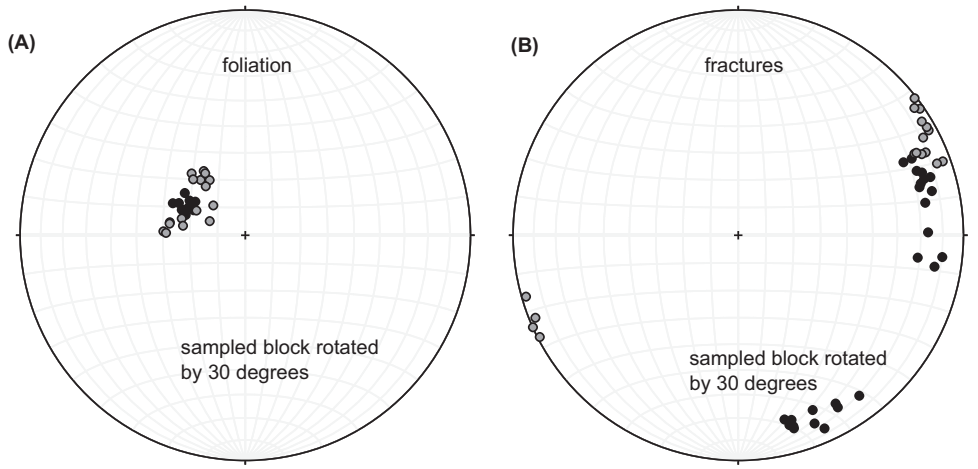


Fig. 3. Stereoplots of the poles for the orientation of (A) foliation and (B) fractures in the bedrock (black dots) and orientation of foliation and fractures in the sampled block of rock (gray dots) after rotation by 30°.

implies that they intersect one another at an approximate angle of 80 degrees. These fractures cut across the gently dipping foliation which is oriented at 027/24. The most conspicuous features of this locality are symmetrical dark halos flanking these fractures (fig. 2). The widest halos have constant widths close to 60 cm. Narrower haloes show discernible tapering upwards (figs. 2 and 4).

## SAMPLING, ANALYTICAL AND COMPUTATIONAL METHODS

### *Sampling*

Samples were collected from a single block measuring approximately 3 m x 5 m x 2 m (width x length x height). This block is dislodged from the cliff face and tilted and rotated with respect to its original orientation by approximately 30 degrees. The block contains six discrete parallel fractures of varying widths (from 0.2–2 cm) of which five are flanked by complete symmetrical dark-colored haloes. The maximum widths of these haloes are 0.2 cm, 3 cm, 14 cm, 20 cm and 60 cm. Stereographic reorientation of this block shows that these fracture-halo systems belong to the same fracture set from the cliff face (fig. 3). Samples were taken and field-based measurements were made on the upper surface of the block. This is because this gently sloping surface was that which was most protected from sea spray and therefore least weathered. Profiles were constructed across the five complete fracture-halo systems. Field-based chemical analyses (see below) were made on all five profiles (profiles 1–5) and samples were taken from the longest of these profiles (profile 5). The width of each halo and the angle at which the haloes taper upwards (which was measured on the sides of the block and other vertical surfaces; table 1) were used to reconstruct the position of each fracture-halo profile along a hypothetical single fracture (fig. 4).

### *Petrography*

Samples from profile 5 were used for petrographic analysis. Mineral modes were estimated by point counting of 1000 evenly spaced points in 17 thin sections from the profile. Point counting was done with a Leica petrographic microscope equipped with an automated stage driven by a PELCON automatic point counter and associated software. Uncertainties were calculated following the approach of Van der Plas and

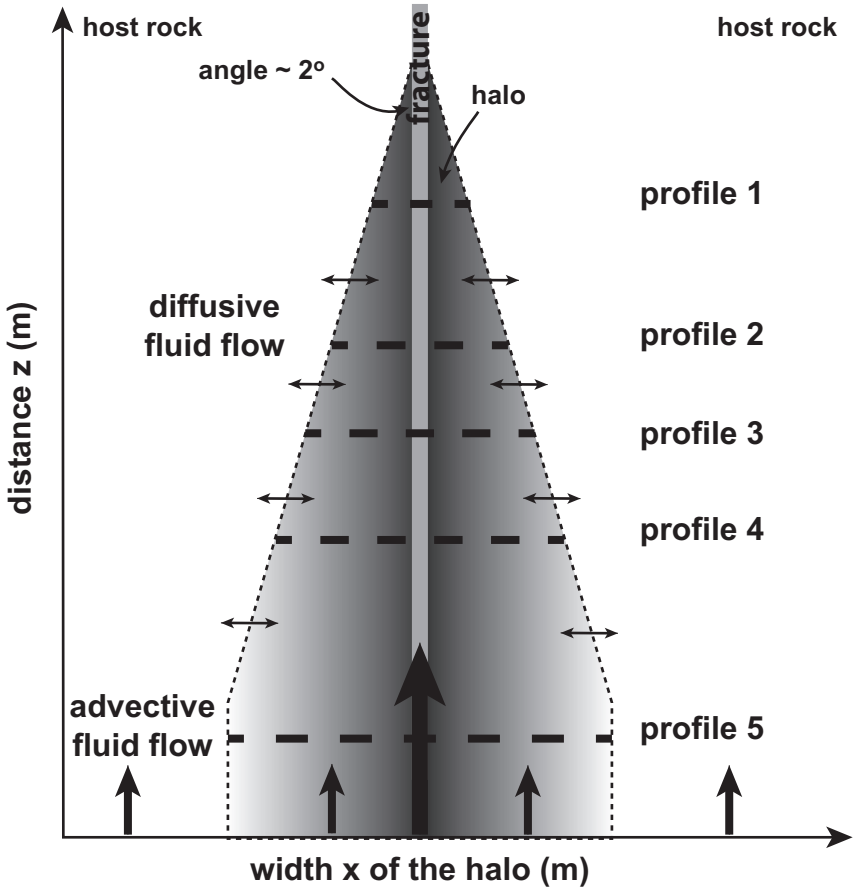


Fig. 4. Reconstruction of the positions of the sampled profiles along a hypothetical fracture.

Tobi (1965). Mineral chemistry was determined using a JEOL JXA-8530 field emission electron microprobe (EMPA) at the Department of Earth Sciences, Uppsala University with running conditions at 15 kV and 20 nA and a beam size of 0.5 to 10 μm.

*Portable XRF-Analysis*

Chemical variation along all five profiles was studied using an Olympus Innov-X Delta handheld XRF analyzer. No drilling is required for this analytical method and chemical analysis is done in the field. The reason for using a portable XRF analyzer was to collect sufficient data so as to better constrain the shape of the geochemical fronts that are to be used for parameterization of metamorphic fluid flow. This field-based method generates a chemical analysis of the rock surface with a penetration depth of 1 to 3 mm (Appendix 1). The spot diameter is 1 cm. One shortcoming of this method is that elements lighter than Mg cannot be analyzed. This is problematic because Na is an important constituent of these rocks. A second shortcoming is that the volume of rock that is analyzed is small compared to the crystal size. This heterogeneity generates scatter in the data that can be partly overcome by reducing sample spacing along each profile. Another way of handling this issue is to use the portable XRF analyzer to study ratios of elements which tend to substitute for one another, rather than absolute

TABLE 1

*Measurements of the vertical distance, width of the halo at the base and at the top as well as measurements of the angle at which vein and haloes narrow upwards of 10 veins at Delfini*

| vein | vertical distance (cm) | width at base (cm) | width at top (cm) | angle at which vein haloes narrow upwards |
|---|---|---|---|---|
| 1 | 50.0 | 38.0 | 35.0 | 3.4 |
| 2 | 60.0 | 30.0 | 25.0 | 4.8 |
| 3 | 90.0 | 15.0 | 10.0 | 3.2 |
| 4 | 200.0 | 10.0 | 5.0 | 1.4 |
| 5 | 100.0 | 4.0 | 2.0 | 1.1 |
| 6 | 170.0 | 2.0 | 1.5 | 0.2 |
| 7 | 250.0 | 10.0 | 5.0 | 1.1 |
| 8 | 250.0 | 25.0 | 12.0 | 3.0 |
| 9 | 90.0 | 33.0 | 32.0 | 0.6 |
| 10 | 120.0 | 1.0 | 0.0 | 0.5 |
| average | | | | 1.9 ± 1.0 |

concentrations of specific elements. This reduces scatter caused by heterogeneous mineral distribution. In our study, we used the ratio Sr/Ca as a measure of the Sr concentration in the rock. This is possible because 1) there is only one modally important calcic phase in the haloes: calcite and 2) there is minimal variation in the calcite mode across the haloes. Sr concentration is a useful tracer of fluid flow, because Sr partitions preferentially into the fluid (Liebscher and others, 2009). A third shortcoming arises because analyses obtained using the field-based method are affected by processes affecting the chemistry of rock surface. The rock surface we studied is largely free from weathering. However, sea salts are precipitated on the rock surface from sea spray and these needed to be subtracted from portable XRF measurements. We were able to remove sea salts from our measurements by assuming that these were NaCl and $Na_2SO_4$ and recalculating accordingly. After handling each of these shortcomings as described, we found that the portable XRF-analyzer was useful for rapidly generating detailed profiles of some elemental ratios. By focusing on the ratio Sr/Ca we were able to gain useful information about fluid-rock interaction from these data.

### *Conventional XRF-Analysis*

Major element concentrations in samples from profile 5 were determined using a Sequential X-Ray Fluorescence (XRF) Rigaku ZSX Primus II Spectrometer at the Department of Geological Sciences at Stockholm University. For XRF-analysis, precision was controlled through repeat analyses of international reference materials (AGV-2) and is better than 1 percent (Appendix 2).

### *Comparison Between Portable and Conventional XRF-Analysis*

In acknowledgement of the above mentioned pitfalls of portable XRF analysis, we compared chemical analyses made by portable and conventional XRF analysis for all data from profile 5 in our study. The comparison shows reasonable agreement between average values and standard deviations for Ca, Sr and Ca/Sr (fig. 5). Further, we note that portable XRF is best suited to analyzing heavier elements (that is from row 4 upwards in the periodic system). Analyses of lighter elements (for example Si and below) tend to be less reliable (Appendix 1).

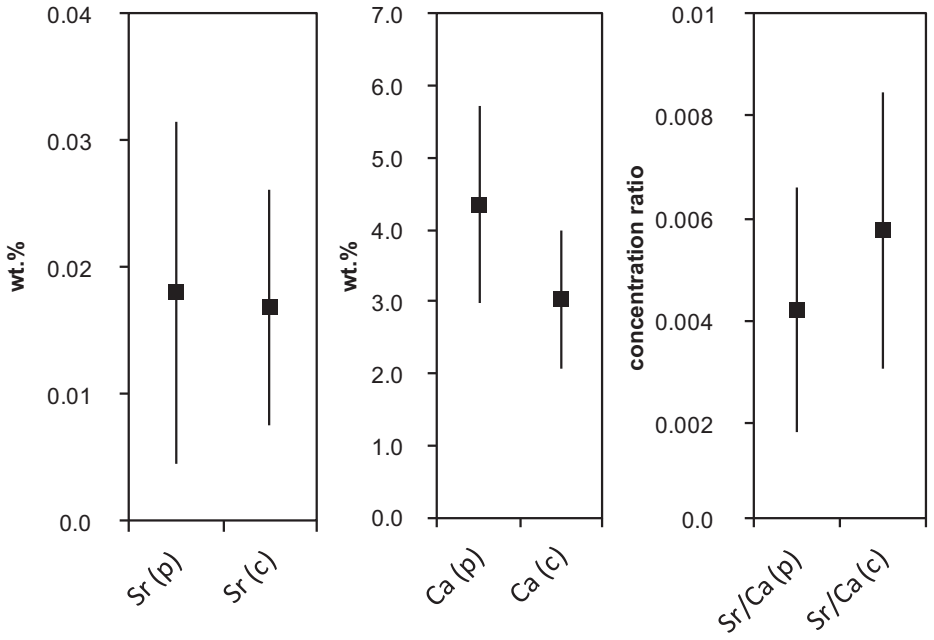


Fig. 5. Comparison of Ca, Sr and Sr/Ca concentrations measured by conventional XRF (c) and by portable XRF (p).

*Analyses of Trace Elements*

For trace element analyses cores of 3 to 5 mm diameter were drilled out of the glass disks that were used for XRF analysis and embedded in epoxy resin. After polishing the glass disks were analyzed by Laser Ablation Inductively Coupled Mass Spectrometry (LA-ICP-MS) using a New Wave 193 excimer laser coupled to a Thermo Xseries2 quadrupole ICP-MS at the PetroTectonics analytical facility at the Department of Geological Sciences, Stockholm University. Analytical conditions included a laser pulse frequency of 10 Hz, a laser energy density of 7 $Jcm^{-2}$ and a spot size of 120 μm. Quantification was performed using Si as internal standard and the international standard reference material (SRM) NIST (National Institute of standards and technology) 612 (Jochum and others, 2011; Appendix 2) was used as external calibration standard with the sample-standard bracketing method. Accuracy was controlled by repeated analysis of the international glass reference material BCR-2G and is better than 5 percent (Appendix 2). Data reduction was performed using the public domain software Iolite (Hellstrom and others, 2008; Paton and others, 2011).

*Modeling of Fluid Flow*

In this section, we model metamorphic fluid flow using the Sr/Ca ratio (monitored by the Sr/Ca ratio) as a tracer. We consider the following flow regime (fig. 4):

- Faster channeled fluid flow along the fracture with pure advective transport of, for example the tracer of interest (here Sr) in the direction of fluid flow (along the fracture).
- Slower pervasive fluid flow in the country rock with pure advective transport in the direction of fluid flow (parallel to the fracture).
- Transverse diffusive transport of the tracer of interest (here Sr) perpendicular to the direction of fluid flow (perpendicular to the fracture).

This flow regime can be expressed mathematically for the fracture and for the surrounding rock by the equations:

$$\frac{\partial c_f}{\partial t} + v\frac{\partial c_f}{\partial z} - \frac{D\theta}{b}\frac{\partial c_r}{\partial x}\Big|_{x=b} = 0 \text{ (fracture)} \tag{1}$$

$$\frac{1}{K_v}\frac{\partial c_r}{\partial t} = D\frac{\partial^2 c_r}{\partial x^2} \text{ (surrounding rock)} \tag{2}$$

where $c_f$ and $c_r$ are the tracer concentrations in the fracture and surrounding rock, respectively; $v$ is the fluid velocity in the fracture; $D$ is the molecular diffusion coefficient of the tracer of interest (here Sr) in the fluid; $b$ is the half fracture aperture; $z$ is the distance along the path of metamorphic fluid flow that is along the fracture; $x$ is the distance perpendicular to this fracture; $K_v$ is the fluid/solid partition coefficient for the tracer of interest (here, Sr); $\theta$ is the porosity of the rock and $t$ is time. In our inverse modeling, equations (1) and (2) are coupled by assuming continuity of concentration along the fracture surface, that is:

$$c_r(z,x = b,t) = c_f(z,t) \tag{3}$$

and we use the following boundary and initial conditions:

$$c_f(z = 0,t) = c_0 \tag{4}$$

which means the tracer concentration $c_0$ at the inlet boundary ($z = 0$);

$$c_f(z,t = 0) = c_{eq} \tag{5}$$

which means the initial tracer concentration $c_{eq}$ in the fracture;

$$c_f(z = \infty,t) = c_{eq} \tag{6}$$

$$c_r(\infty,x,t) = c_{eq} \tag{7}$$

which means the tracer concentration in downstream of the geochemical front ($z = \infty$);

$$c_r(z,x,0) = c_{eq} \tag{8}$$

which means $t$ the initial tracer concentration $c_{eq}$ in the matrix.
Given the following transformations to dimensionless variables:

$$x' = \frac{x}{h} \tag{9}$$

$$z' = \frac{z}{h} \tag{10}$$

$$c_{f'} = \frac{c_f - c_{eq}}{c_0 - c_{eq}} \tag{11}$$

$$c_{r'} = \frac{c_r - c_{eq}}{c_0 - c_{eq}} \tag{12}$$

$$t' = \frac{vt}{h} \tag{13}$$

Equations (1)–(8) become:

$$\frac{\partial c_{f'}}{\partial t'} + \frac{\partial c_{f'}}{\partial z'} - \frac{D_e}{\nu b}\frac{\partial c_{r'}}{\partial x'}\Big|_{\partial x' = b/h} = 0 \text{ (fracture)} \tag{14}$$

$$\frac{\partial c_{r'}}{\partial t'} = \frac{K_v D_e}{\nu \theta h}\frac{\partial^2 c_{r'}}{\partial x'^2} \text{ (surrounding rock)} \tag{15}$$

$$c_{r'}(z', x' = b/h, t') = c_{f'}(z', t') \tag{16}$$

$$c_{f'}(z' = 0, t') = 1 \tag{17}$$

$$c_{f'}(z', t' = 0) = 0 \tag{18}$$

$$c_{f'}(z' = \infty, t') = 0 \tag{19}$$

$$c_{r'}(\infty, x', t') = 0 \tag{20}$$

$$c_{r'}(z', x', 0) = 0 \tag{21}$$

The solutions to equations (14) and (15) for tracer concentrations in the fracture and country rock are (Neretnieks and others, 1982):

$$c_{f'} = erfc\left(\frac{\frac{z\theta}{b}\left(\frac{Dh}{\nu K_v}\right)^{0.5}}{2(t - z/h)^{0.5}}\right) \tag{22}$$

$$c_{r'} = erfc\left(\frac{\frac{z\theta}{b}\left(\frac{Dh}{\nu K_v}\right)^{0.5} + (x - b/h)\left(\frac{\nu h}{K_v D}\right)^{0.5}}{2(t - z/h)^{0.5}}\right) \tag{23}$$

where $t$ should be larger than $z$.

## RESULTS

### *Petrography*

The country rock can be classified as a quartz-mica schist metamorphosed at greenschist facies conditions (Keiter and others, 2011). Elsewhere at Delfini some blueschist facies minerals are preserved but these were not seen in our samples. Conjugate fractures contain coarse-grained quartz and calcite. Vein mineralogy is similar for all veins studied at Delfini. These fractures are rimmed by conspicuous haloes that are darker than the country rock. The boundaries between the unaltered country rock and the halos are sharp. In the field the bounds of the halos are easily distinguished on the basis of their dark green color compared with the light green country rock (fig. 2). Whole rock bulk analyses show that the extension of each dark halo corresponds with the parts of the halo that show a distinct increase of the volatile content (fig. 9). We therefore use volatile content that was measured as loss on ignition (LOI) to define the boundaries between the country rock and the halos.

### *Mineral Modes, Chemistry and Reaction Textures*

Mineral modes are listed in table 2 and shown graphically in figure 6. Mineral chemistry data are listed in table 3. The country rock is dominantly composed of white mica, albite, clinopyroxene and quartz with minor amounts of calcite, epidote, Fe-oxides and accessory titanite and allanite. White mica is of phengitic composition with Si (in cation per formula unit; c.p.f.u.) ~3.5 and $X_{Mg}$ ~0.6 with $X_{Mg}$=Mg/(Mg+Fe). Phengite defines the penetrative foliation of the country rock. It is the most

TABLE 2

*Mineral modes for profile 5*

| sample | -0.4DEI | -0.35DEI | -0.3DEI | -0.25DEI | -0.2DEI | -0.15DEI | -0.1DEI | -0.05DEI | 0.0DEI | 0.15DEI | 0.2DEI | 0.25DEI | 0.27DEI | 0.3DEI | 0.35DEI | 0.4DEI | 0.45DEI |
|---|---|---|---|---|---|---|---|---|---|---|---|---|---|---|---|---|---|
| distance (m) | -0.4 | -0.35 | -0.3 | -0.25 | -0.2 | -0.15 | -0.1 | -0.05 | 0.0 | 0.15 | 0.2 | 0.25 | 0.27 | 0.3 | 0.35 | 0.4 | 0.45 |
| comment | country rock | | | halo | | | | | | | | | | country rock | | | |
| white mica | 53.1 | 46.7 | 47.9 | 46.5 | 46.1 | 40.9 | 39.8 | 32.0 | 35.7 | 37.3 | 43.3 | 47.6 | 42.9 | 49.0 | 50.1 | 47.8 | 50.4 |
| albite | 16.8 | 14.3 | 14.3 | 22.3 | 22.8 | 26.1 | 25.1 | 25.2 | 34.0 | 30.3 | 18.2 | 22.2 | 18.1 | 17.7 | 20.7 | 19.1 | 12.9 |
| quartz | 11.9 | 13.0 | 14.3 | 8.5 | 11.6 | 8.4 | 11.7 | 21.8 | 5.2 | 7.3 | 17.2 | 11.7 | 15.7 | 9.9 | 14.5 | 9.4 | 12.9 |
| amphibole | 13.5 | 10.4 | 10.4 | 4.6 | 0.0 | 0.0 | 0.0 | 0.0 | 0.0 | 0.0 | 0.7 | 2.0 | 3.8 | 12.5 | 12.9 | 13.9 | 14.3 |
| sphene | 0.5 | 0.8 | 0.3 | 0.8 | 0.7 | 0.3 | 1.2 | 0.3 | 0.2 | 0.9 | 0.7 | 0.6 | 0.3 | 0.0 | 0.0 | 0.2 | 0.6 |
| Fe-oxides | 0.0 | 0.0 | 0.0 | 2.0 | 1.7 | 3.2 | 1.8 | 1.9 | 3.0 | 2.1 | 2.4 | 2.9 | 2.3 | 0.4 | 0.3 | 0.3 | 0.0 |
| epidote | 1.6 | 2.3 | 2.0 | 0.0 | 0.0 | 0.0 | 0.0 | 0.0 | 0.0 | 0.0 | 0.0 | 1.6 | 1.5 | 3.7 | 2.1 | 1.6 | 1.4 |
| calcite | 2.6 | 5.7 | 5.5 | 9.2 | 5.8 | 6.1 | 7.9 | 7.3 | 0.0 | 8.2 | 7.3 | 6.9 | 11.2 | 5.4 | 1.2 | 7.2 | 1.9 |
| allanite | 0.0 | 0.0 | 0.0 | 0.0 | 0.0 | 0.9 | 0.0 | 0.0 | 0.0 | 0.0 | 0.5 | 0.0 | 0.1 | 0.0 | 0.0 | 0.0 | 0.0 |
| biotite | 0.0 | 0.0 | 0.0 | 6.1 | 11.3 | 14.1 | 12.5 | 10.4 | 2.2 | 13.9 | 9.7 | 4.5 | 4.1 | 0.0 | 0.0 | 0.0 | 0.0 |
| chlorite | 0.0 | 0.0 | 0.0 | 0.0 | 0.0 | 0.0 | 0.0 | 1.2 | 19.7 | 0.0 | 0.0 | 0.0 | 0.0 | 0.0 | 0.0 | 0.0 | 0.0 |

Note, that distances are outgoing from the edge of the veins on both sides.

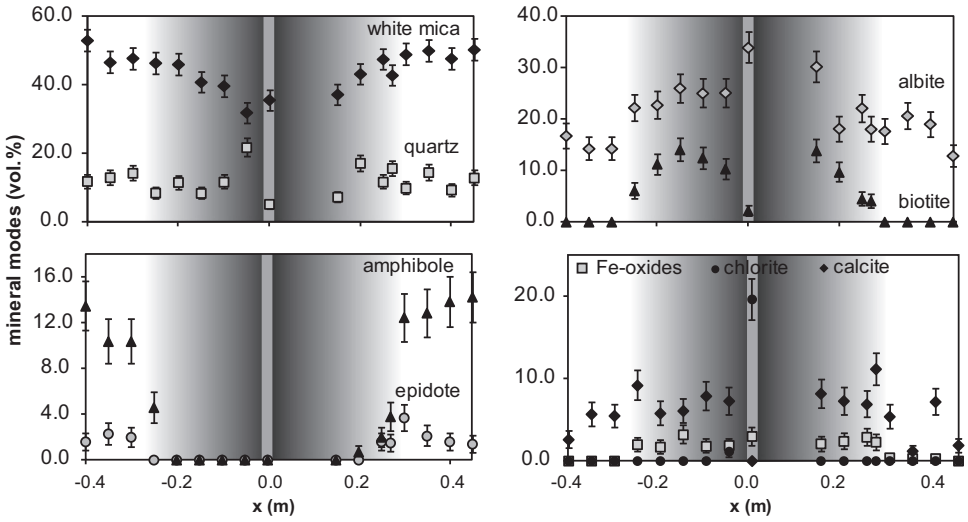


Fig. 6. Mineral modes along profile 5.

abundant mineral in the country rock with an average mode of ~50 volume percent. Its mode decreases in the halo towards the fracture reaching a minimum of ~30 volume percent. Within the halo, calcite gradually replaces phengite which grows along its cleavage and the rims (fig. 7A). Epidote with $X_{cz}$ ~0.04 with $X_{cz}$=(Al-2)/(Al+$Fe^{3+}$+$Cr^{3+}$-2) (after Franz and Liebscher, 2004) only occurs as small grains in the country rock (~2 vol.%) and is completely replaced by biotite and calcite in the halo (fig. 7B). Clinopyroxene from the country rock and halo can be classified as omphacite with $X_{jadeite}$ ~0.45 (after Morimoto, 1988). Omphacite appears as porphyroblasts (up to 1.5 mm) which are embedded into the foliation (fig. 8A). Omphacite is most abundant in the country rock (~10 vol.%) and mineral modes decrease abruptly at the boundary between country rock and halo. Omphacite is completely absent close to the fracture and pseudomorphically replaced by calcite and fine-grained biotite in the halo (figs. 8B and 8C). Cuboidal Fe-oxides (mostly altered to hematite) grow randomly within these pseudomorphic relicts. Biotite ($X_{Fe}$ ~0.5 with $X_{Fe}$=Fe/(Fe+Mg)) is found only in the halo. It appears as a fine-grained replacement product after omphacite (figs. 8B and 8C). The mineral modes of biotite increase systematically from the outer parts of the halo (~4 vol.%) towards the fracture (~15 vol.%). Immediately adjacent to the fracture, biotite modes decrease dramatically to 2 volume percent which can be explained by the replacement of biotite by chlorite (fig. 7C). Chlorite is slightly Mg enriched ($X_{Mg}$ ~0.6) and its abundance is much higher adjacent to the fracture (~20 vol.%) than elsewhere (~1 vol.%). Albite ($X_{Ab}$ ~1.0 with $X_{Ab}$=Na/(Na+K+Ca)) occurs interstitially and replacing phengite and omphacite (fig. 8D). Albite is most abundant in the halo closest to the fracture (~35 vol.%). Quartz occurs as small interstitial crystals throughout the profile.

### *Chemical Variation Measured by Conventional XRF*

Chemical data obtained by conventional XRF are listed in table 4 and shown graphically in figures 9, 10 and 11. Little to no significant variation in concentrations of major elements such as $SiO_2$ (~60 wt.%), $Al_2O_3$ (~17 wt.%), CaO (~4 wt.%), MgO (~3 wt.%), $TiO_2$ (~0.7 wt.%) and $Fe_2O_3$ (~6 wt.%) is observed in the halo and country rock (fig. 9). Significant variation in concentration could be observed in the

TABLE 3

*Microprobe data of representative minerals from profile 5*

| sample<br>mineral | -0.01DE-1<br>chlorite | 0.2DE-1<br>albite | 0.15DE-1<br>biotite | 0.4DE-1<br>phengite | 0.4DE-1<br>clinopyroxene | 0.4DE-1<br>epidote | 0.15DE-1<br>Fe-oxide |
|---|---|---|---|---|---|---|---|
| $SiO_2$ | 28.50 | 69.90 | 40.07 | 52.96 | 55.18 | 37.50 | 0.23 |
| $TiO_2$ | 0.08 | 0.00 | 1.51 | 0.06 | 0.04 | 0.03 | 1.11 |
| $Al_2O_3$ | 19.29 | 19.66 | 13.79 | 25.01 | 9.37 | 21.17 | 0.11 |
| Cr2O3 | n.d. | n.d. | 0.08 | 0.02 | 0.02 | 0.02 | 0.03 |
| FeO | 22.21 | n.d. | 18.33 | 4.10 | 12.67 | 13.41 | 86.87 |
| MnO | 0.18 | n.d. | 0.15 | 0.05 | 0.39 | 0.16 | n.d. |
| MgO | 17.85 | n.d. | 12.93 | 3.47 | 3.42 | 0.01 | 0.05 |
| CaO | 0.06 | n.d. | 0.04 | 0.15 | 11.40 | 22.24 | 0.03 |
| $Na_2O$ | n.d. | 10.15 | 0.15 | 0.07 | 7.39 | n.d. | n.d. |
| $K_2O$ | 0.11 | 0.05 | 9.27 | 9.64 | 0.06 | 0.01 | 0.01 |
| NiO | - | - | - | - | - | - | 0.01 |
| $V_2O_3$ | - | - | - | - | - | - | 0.20 |
| Total | 88.27 | 99.76 | 96.32 | 95.51 | 99.95 | 94.56 | 88.44 |
| Si | 2.92 | 3.03 | 2.98 | 3.53 | 2.03 | 3.06 | 0.01 |
| Ti | 0.01 | | 0.08 | 0.003 | 0.001 | 0.002 | 0.02 |
| Al | 2.33 | 1.01 | 1.21 | 1.96 | 0.41 | 2.03 | 0.003 |
| Cr | 0.004 | 0.001 | 0.001 | 0.001 | 0.001 | | |
| $Fe^{2+}$ | 1.90 | | 1.14 | 0.23 | 0.32 | | |
| $Fe^{3+}$ | | | | | 0.07 | 0.91 | 1.95 |
| Mn | 0.02 | | 0.01 | 0.003 | 0.01 | 0.01 | |
| Mg | 2.73 | | 1.44 | 0.34 | 0.19 | 0.001 | 0.002 |
| Ca | 0.01 | | 0.003 | 0.01 | 0.45 | 1.94 | 0.001 |
| Na | | 0.85 | 0.02 | 0.01 | 0.53 | | |
| K | 0.01 | 0.003 | 0.88 | 0.82 | 0.003 | 0.001 | < 0.001 |
| Ni | | | | | | | < 0.001 |
| V | | | | | | | 0.01 |
| Total | 9.92 | 4.89 | 7.78 | 6.90 | 4.00 | 7.97 | 2.00 |
| $X_{Mg}$ | 0.59 | | 0.56 | 0.60 | 0.37 | | |
| $X_{Fe}$ | 0.41 | | 0.44 | | | | |
| $X_{an}$ | | 0.00 | | | | | |
| $X_{ab}$ | | 0.997 | | | | | |
| $X_{or}$ | | 0.003 | | | | | |
| $X_{cz}$ | | | | | | | |
| $X_{jd}$ | | | | | 0.45 | 0.04 | |
| $X_{ae}$ | | | | | 0.07 | | |
| $X_{di}$ | | | | | 0.55 | | |

n.d. = not detected.

volatile content (measured as loss on ignition) which corresponds to the amount of $H_2O$ and $CO_2$, and in the concentrations of $Na_2O$ and $K_2O$ (fig. 9). The volatile content is higher (~4.5 wt.%) in the halos than in the country rock (~3 wt.%). The concentration of $K_2O$ decreases gradually from 6 to 5 weight percent towards the fracture while the concentration of $Na_2O$ increases from 3 to 4 weight percent towards the fracture.

### *Mass Balance Calculations*

Mass balance calculations have been carried out by combining the different approaches described of Baumgartner and Olsen (1995), Penniston-Dorland and Ferry (2008) and Ague (2011). To observe true mass changes during metamorphic and/or metasomatic events and to eliminate primary compositional variations, major and trace elements can be normalized to an immobile reference element. Instead of using only one single immobile reference element it has been suggested to use a so

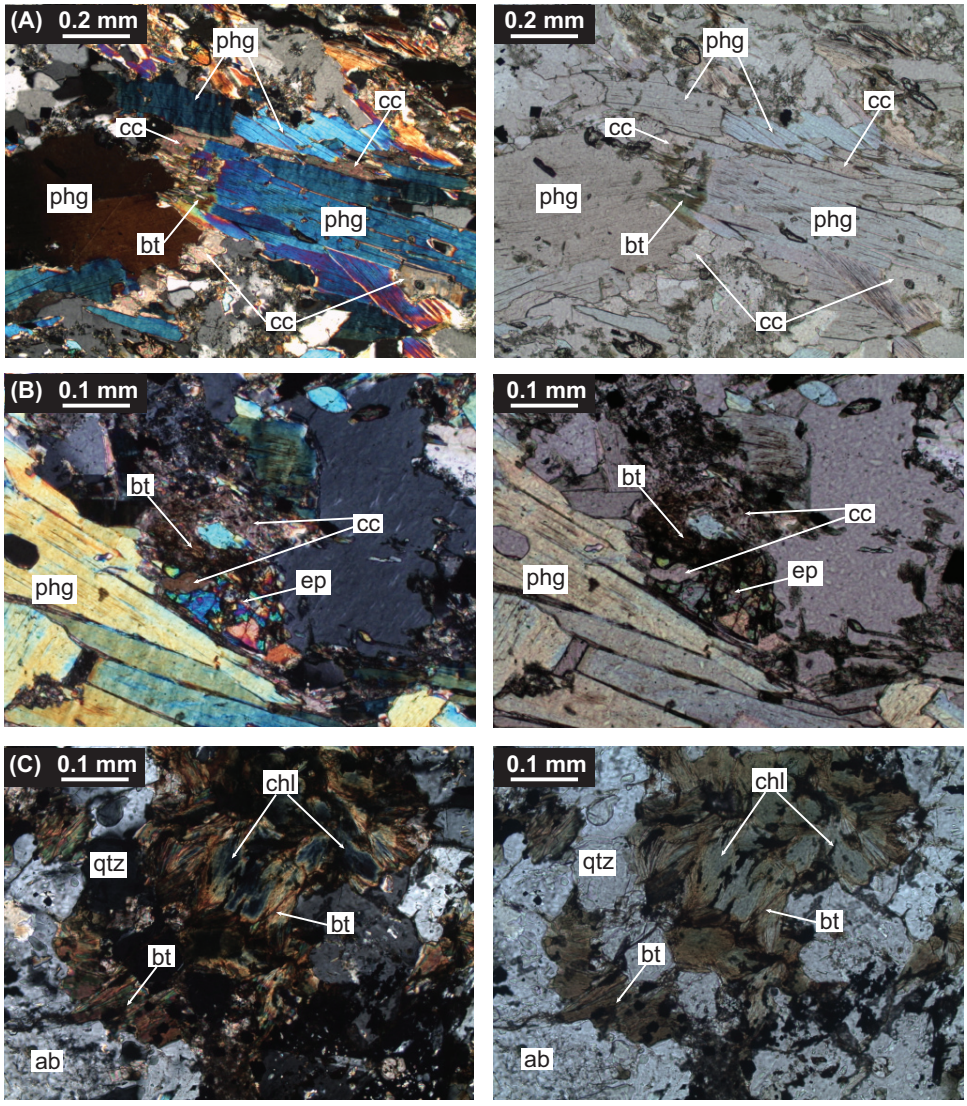


Fig. 7. Microphotographs. (A) Rimming and replacement of phengite by calcite and biotite. (B) Replacement of epidote by calcite and biotite. (C) Replacement of biotite by chlorite. ab = albite; bt = biotite; cc = calcite; chl = chlorite; ep = epidote; phg = phengite; qtz = quartz.

called immobile or geochemical reference frame which involves several immobile species (Baumgartner and Olsen, 1995; Ague and van Haren, 1996; Penniston-Dorland and Ferry, 2008; Ague, 2011). In this study, overlapping concentration ratios (altered concentration/unaltered concentration) of several elements were used to determine the immobile reference frame (after Baumgartner and Olsen, 1995). For this purpose elements that occur in minerals within the vein were excluded (here: Si and Ca). Further, elements that are considered to be mobile under metamorphic conditions (for example K, Na, Ca, Fe, Mg, Mn, Al, P, Rb, Ba, Cs, Sr) were also avoided (Shaw, 1954, 1956; Tanner and Miller, 1980; Ferry, 1983; Ague, 1994a, 2003a, 2011; Penniston-Dorland and Ferry, 2008). Elements that were considered suitable for the immobile

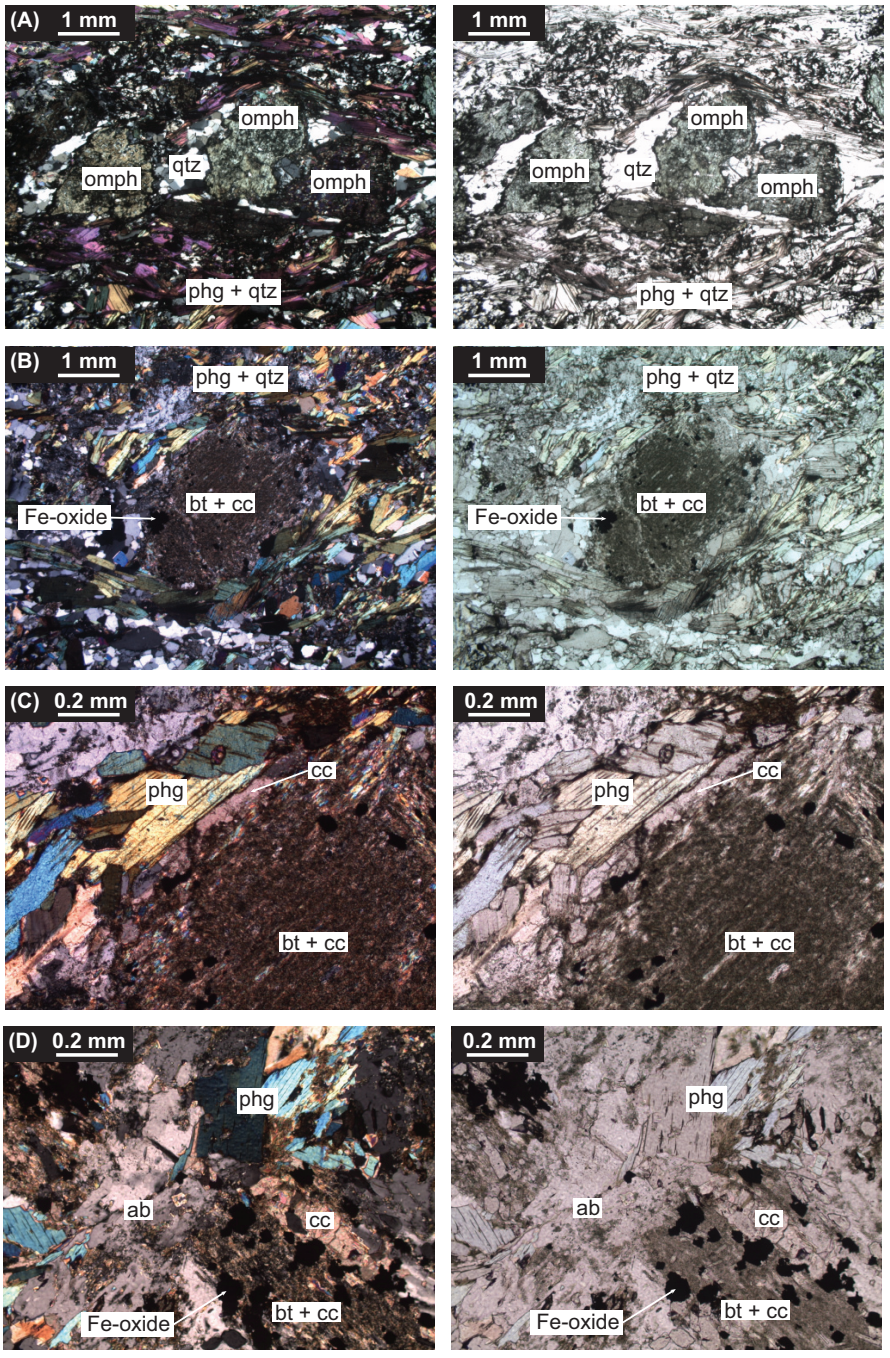


Fig. 8. Microphotographs. (A) Porphyroblasts of omphacite embedded in foliation. (B) Replacement of omphacite by fine-grained biotite and hematite. (C) Replacement of omphacite by calcite and biotite. (D) Replacement of relicts of omphacite and phengite by albite. ab = albite; bt = biotite; cc = calcite; phg = phengite; qtz = quartz; omph = omphacite.

TABLE 4

*Chemical data obtained by conventional XRF (major elements) and LA-ICP-MS (trace elements) for profile 5*

| sample | -0.4DEI | -0.35DEI | -0.3DEI | -0.25DEI | -0.2DEI | -0.15DEI | -0.1DEI | -0.05DEI | -0.01DEI | 0.0-DEI | 0.02-DEI | 0.15DEI | 0.2DEI | 0.25DEI | 0.27DEI | 0.3DEI | 0.35DEI | 0.4DEI | 0.45DEI |
|---|---|---|---|---|---|---|---|---|---|---|---|---|---|---|---|---|---|---|---|
| distance (m) | -0.4 | -0.35 | -0.3 | -0.25 | -0.2 | -0.15 | -0.1 | -0.05 | -0.01 | 0 | 0.02 | 0.15 | 0.2 | 0.25 | 0.27 | 0.3 | 0.35 | 0.4 | 0.45 |
| comment | country rock | | | halo | | | | | | | | | | | | country rock | | | |
| *major elements (wt.%)* | | | | | | | | | | | | | | | | | | | |
| $SiO_2$ | 60.2 | 58.7 | 58.5 | 60.3 | 59.4 | 59.7 | 59.7 | 57.9 | 58.6 | 62.2 | 59.2 | 60.6 | 60.3 | 59.8 | 62.1 | 60.8 | 60.7 | 60.2 | 60.4 |
| $Al_2O_3$ | 17.0 | 17.6 | 17.4 | 16.6 | 17.0 | 17.0 | 16.9 | 17.6 | 15.4 | 17.5 | 16.6 | 16.7 | 16.8 | 17.4 | 16.0 | 17.1 | 17.1 | 16.9 | 17.5 |
| CaO | 4.3 | 4.6 | 4.9 | 4.4 | 4.2 | 4.0 | 4.0 | 4.3 | 8.9 | 1.6 | 4.9 | 4.1 | 3.9 | 3.6 | 3.8 | 3.6 | 3.7 | 4.4 | 3.3 |
| MgO | 2.7 | 2.8 | 2.8 | 2.9 | 3.0 | 3.0 | 3.0 | 3.1 | 2.3 | 2.6 | 2.8 | 2.9 | 3.0 | 2.9 | 2.8 | 2.6 | 2.7 | 2.6 | 2.7 |
| MnO | 0.09 | 0.09 | 0.09 | 0.10 | 0.11 | 0.10 | 0.10 | 0.10 | 0.15 | 0.11 | 0.11 | 0.09 | 0.11 | 0.10 | 0.11 | 0.10 | 0.10 | 0.10 | 0.09 |
| $P_2O_5$ | 0.4 | 0.4 | 0.4 | 0.4 | 0.4 | 0.4 | 0.4 | 0.4 | 0.4 | 0.4 | 0.4 | 0.3 | 0.4 | 0.4 | 0.4 | 0.4 | 0.4 | 0.4 | 0.4 |
| $^1Fe_2O_3$(tot) | 6.0 | 6.3 | 6.4 | 6.2 | 6.4 | 6.2 | 6.3 | 6.4 | 5.4 | 5.6 | 6.2 | 5.8 | 6.2 | 6.1 | 5.9 | 6.1 | 6.0 | 6.0 | 6.1 |
| $Na_2O$ | 3.1 | 2.6 | 2.5 | 2.6 | 2.9 | 3.0 | 3.2 | 3.8 | 4.4 | 4.9 | 4.3 | 3.3 | 2.7 | 2.9 | 2.1 | 3.0 | 2.8 | 2.9 | 2.8 |
| $K_2O$ | 5.7 | 6.2 | 6.2 | 6.0 | 6.1 | 5.9 | 5.7 | 5.7 | 3.8 | 4.5 | 4.7 | 5.5 | 6.1 | 6.1 | 6.1 | 5.7 | 5.9 | 5.9 | 6.1 |
| $TiO_2$ | 0.7 | 0.7 | 0.7 | 0.7 | 0.6 | 0.7 | 0.7 | 0.7 | 0.6 | 0.7 | 0.7 | 0.6 | 0.7 | 0.7 | 0.6 | 0.6 | 0.6 | 0.6 | 0.7 |
| LOI | 3.1 | 3.8 | 4.2 | 4.7 | 4.7 | 4.7 | 4.5 | 4.8 | 7.9 | 2.8 | 5.2 | 4.7 | 4.5 | 4.2 | 4.2 | 2.9 | 3.0 | 3.5 | 3.1 |
| *trace elements (ppm)* | | | | | | | | | | | | | | | | | | | |
| V | 162 | 141 | 171 | 169 | 152 | 143 | 154 | 164 | 149 | 170 | 138 | 136 | 163 | 163 | 134 | 135 | 135 | 139 | 147 |
| Rb | 209 | 193 | 227 | 233 | 219 | 195 | 212 | 213 | 144 | 176 | 152 | 192 | 233 | 222 | 190 | 171 | 189 | 186 | 207 |
| Sr | 328 | 349 | 385 | 186 | 104 | 74 | 87 | 93 | 161 | 81 | 87 | 231 | 174 | 155 | 141 | 131 | 153 | 140 | 146 |
| Y | 23.6 | 22.0 | 25.1 | 22.7 | 19.5 | 17.3 | 18.0 | 20.0 | 41.4 | 14.4 | 18.3 | 15.2 | 27.2 | 21.2 | 16.9 | 18.2 | 18.1 | 19.1 | 20.7 |
| Zr | 276 | 293 | 326 | 288 | 312 | 255 | 234 | 279 | 269 | 268 | 268 | 252 | 373 | 277 | 230 | 267 | 253 | 254 | 279 |
| Nb | 67.0 | 60.0 | 69.0 | 65.0 | 63.0 | 57.0 | 59.0 | 64.3 | 67.3 | 64.3 | 57.5 | 53.7 | 67.7 | 65.0 | 50.3 | 52.3 | 54.9 | 55.7 | 62.0 |
| Cs | 1.9 | 1.9 | 2.2 | 3.6 | 3.4 | 3.7 | 5.3 | 4.6 | 2.4 | 3.6 | 3.0 | 4.5 | 3.5 | 3.6 | 2.7 | 1.5 | 1.6 | 1.7 | 1.8 |
| Ba | 743 | 693 | 837 | 700 | 737 | 637 | 670 | 680 | 537 | 533 | 495 | 607 | 720 | 693 | 597 | 640 | 667 | 663 | 717 |
| La | 57.3 | 92.0 | 80.3 | 93.7 | 60.7 | 51.9 | 71.0 | 72.7 | 109.0 | 41.3 | 59.5 | 70.0 | 143.7 | 118.3 | 53.3 | 55.0 | 53.4 | 51.0 | 63.7 |
| Ce | 122 | 165 | 140 | 170 | 116 | 102 | 128 | 130 | 169 | 89 | 111 | 132 | 220 | 210 | 101 | 102 | 102 | 92 | 119 |
| Pr | 13.1 | 15.0 | 14.3 | 16.9 | 11.5 | 10.1 | 12.6 | 13.4 | 19.2 | 10.0 | 11.0 | 11.9 | 22.1 | 19.0 | 10.0 | 10.1 | 9.9 | 9.5 | 11.9 |
| Nd | 49.8 | 54.7 | 51.2 | 60.0 | 43.8 | 36.4 | 45.4 | 48.3 | 69.7 | 39.0 | 41.2 | 43.8 | 76.0 | 61.0 | 35.2 | 38.4 | 36.2 | 36.2 | 43.9 |
| Sm | 9.2 | 8.4 | 8.5 | 9.3 | 7.7 | 6.3 | 7.4 | 7.4 | 12.1 | 6.9 | 6.9 | 6.3 | 12.1 | 9.1 | 5.7 | 6.3 | 6.2 | 6.4 | 7.6 |
| Gd | 6.1 | 6.0 | 6.1 | 6.3 | 5.4 | 4.5 | 5.1 | 5.8 | 9.3 | 4.8 | 5.0 | 4.6 | 7.3 | 6.1 | 4.3 | 4.5 | 4.6 | 4.8 | 5.2 |
| Tb | 0.8 | 0.7 | 0.8 | 0.8 | 0.7 | 0.6 | 0.6 | 0.8 | 1.4 | 0.6 | 0.7 | 0.6 | 0.9 | 0.8 | 0.6 | 0.6 | 0.6 | 0.7 | 0.7 |
| Dy | 4.7 | 4.4 | 5.0 | 4.6 | 4.4 | 3.4 | 3.9 | 4.2 | 7.6 | 3.4 | 3.9 | 3.2 | 5.6 | 4.6 | 3.5 | 3.7 | 3.5 | 3.8 | 4.2 |
| Ho | 0.9 | 0.9 | 1.0 | 0.9 | 0.8 | 0.7 | 0.7 | 0.7 | 1.6 | 0.6 | 0.7 | 0.6 | 1.0 | 0.8 | 0.6 | 0.7 | 0.7 | 0.7 | 0.8 |
| Er | 2.4 | 2.4 | 2.5 | 2.5 | 2.3 | 1.8 | 1.9 | 2.3 | 4.2 | 1.5 | 2.0 | 1.6 | 2.6 | 2.3 | 1.8 | 2.0 | 1.9 | 2.0 | 2.2 |

TABLE 4

*(continued)*

| sample | -0.4DEI | -0.35DEI | -0.3DEI | -0.25DEI | -0.2DEI | -0.15DEI | -0.1DEI | -0.05DEI | -0.01DEI | 0.0-DEI | 0.02-DEI | 0.15DEI | 0.2DEI | 0.25DEI | 0.27DEI | 0.3DEI | 0.35DEI | 0.4DEI | 0.45DEI |
|---|---|---|---|---|---|---|---|---|---|---|---|---|---|---|---|---|---|---|---|
| distance (m) | -0.4 | -0.35 | -0.3 | -0.25 | -0.2 | -0.15 | -0.1 | -0.05 | -0.01 | 0 | 0.02 | 0.15 | 0.2 | 0.25 | 0.27 | 0.3 | 0.35 | 0.4 | 0.45 |
| comment | country rock | | | halo | | | | | | | | | | | | country rock | | | |
| *trace elements (ppm)* | | | | | | | | | | | | | | | | | | | |
| Tm | 0.4 | 0.4 | 0.4 | 0.4 | 0.4 | 0.3 | 0.3 | 0.3 | 0.5 | 0.2 | 0.3 | 0.3 | 0.4 | 0.4 | 0.3 | 0.3 | 0.3 | 0.3 | 0.3 |
| Yb | 2.6 | 2.4 | 2.8 | 2.5 | 2.2 | 2.0 | 2.1 | 2.4 | 3.8 | 1.5 | 2.2 | 1.7 | 2.9 | 2.4 | 1.8 | 2.1 | 2.1 | 2.1 | 2.4 |
| Lu | 0.4 | 0.4 | 0.4 | 0.4 | 0.3 | 0.3 | 0.3 | 0.3 | 0.5 | 0.2 | 0.3 | 0.3 | 0.4 | 0.4 | 0.3 | 0.3 | 0.3 | 0.3 | 0.3 |
| Hf | 6.1 | 6.4 | 7.0 | 6.3 | 7.2 | 5.6 | 5.0 | 6.2 | 5.9 | 5.9 | 5.9 | 5.2 | 8.1 | 6.1 | 5.2 | 5.7 | 5.2 | 5.6 | 6.0 |
| Ta | 3.3 | 3.1 | 3.4 | 3.3 | 3.5 | 3.0 | 3.1 | 3.3 | 3.3 | 3.3 | 3.0 | 2.6 | 3.7 | 3.3 | 2.5 | 2.7 | 2.8 | 2.8 | 3.1 |
| Pb | 6.5 | 7.1 | 6.4 | 3.4 | 2.9 | 3.0 | 6.7 | 23.8 | 73.3 | 19.6 | 31.0 | 9.3 | 5.1 | 6.8 | 3.7 | 2.6 | 3.9 | 3.4 | 4.8 |
| Th | 20.4 | 20.9 | 21.8 | 23.0 | 22.1 | 16.6 | 19.0 | 20.7 | 21.6 | 18.4 | 17.5 | 19.0 | 28.0 | 22.4 | 15.3 | 17.3 | 17.3 | 16.7 | 18.8 |
| U | 4.0 | 4.1 | 4.3 | 4.1 | 3.2 | 3.1 | 3.4 | 4.4 | 5.0 | 4.6 | 4.6 | 2.9 | 3.8 | 4.8 | 3.0 | 3.1 | 3.2 | 3.1 | 3.9 |
| [2]wRE | 2.004 | 2.054 | 2.211 | 2.095 | 2.185 | 1.843 | 1.837 | 2.041 | 2.010 | 1.953 | 1.921 | 1.766 | 2.476 | 2.066 | 1.660 | 1.813 | 1.770 | 1.796 | 1.966 |

Note, that distances are outgoing from the edge of the veins on both sides.
[1] $Fe_2O_3$(tot) = total iron.
[2] wRE was calculated after Ague (2011).

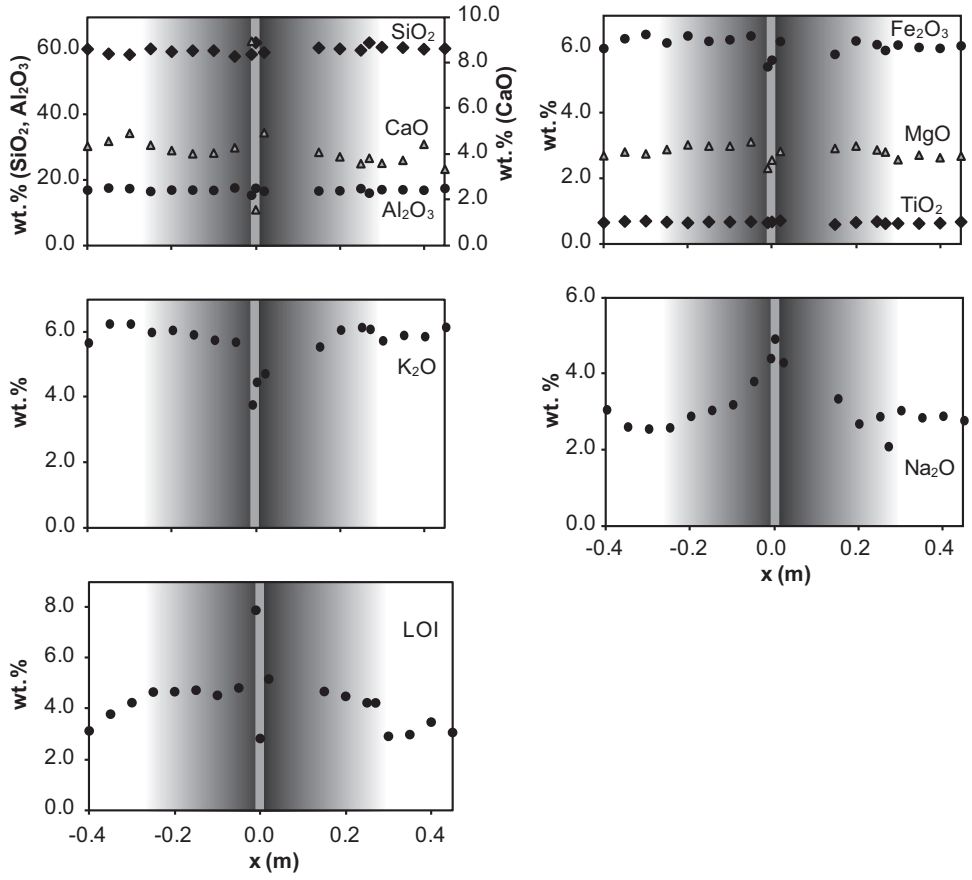


Fig. 9. Variations in concentrations of major elements and the volatile content (measured in loss on ignition = LOI) along profile 5.

reference frame were Ti, Zr, Hf, Ta and Th after following the method described by Baumgartner and Olsen (1995). The concentrations of these immobile elements were further used to calculate a weighted sum of reference species concentrations (wRE) as described by Ague (2011). The obtained wRE values (table 4) were thereafter used to calculate the mass change percentages for the halo that are shown in figure 10 (after Ague, 2011).

The overall mass change in the halo occurred within generally mobile elements such as Cs, Pb, K, Na and Sr. No significant mass change has been observed in concentrations of major elements such as Si, Al, Mg, and Fe and the HFSEs.

To observe mass changes along the profile, concentrations of trace elements have been normalized to Ti and have been plotted against distance from the fracture (fig. 9). Variations in the concentrations of more mobile trace elements such as Cs, Ba, Pb and Sr could be seen (fig. 11) whereas concentration of the HFSEs and other immobile trace elements do not vary throughout the profile (table 4). The Ti-normalized concentration of Pb is higher in and close to the fracture whereas the concentration of Cs is higher throughout the halo. In contrast, concentrations of Ba and Sr are lower in the halo than in the country rock (fig. 11). In summary both alkali and alkaline earth

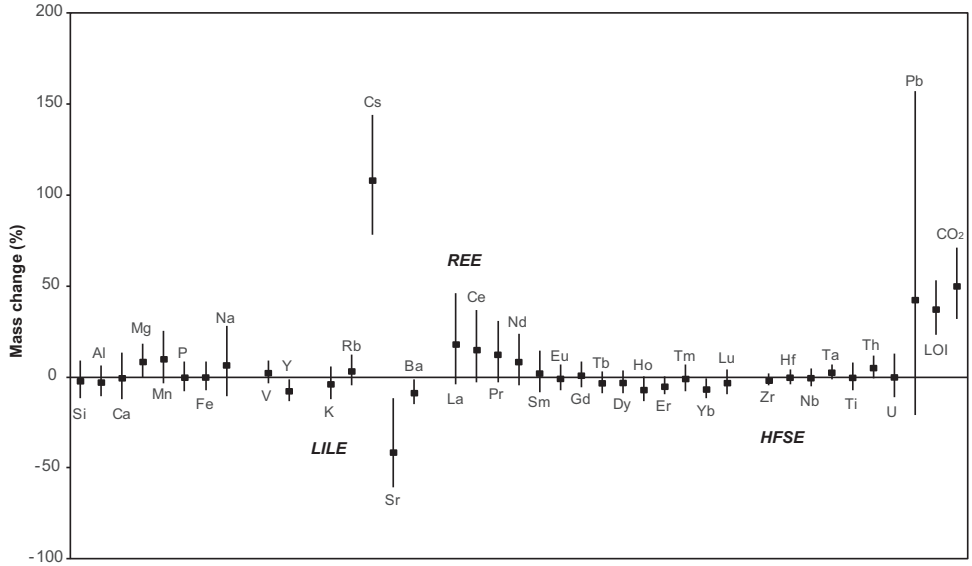


Fig. 10. Mass change percentage of analyzed element concentrations from profile 5 calculated by following the mass balance approaches of Baumgartner and Olsen (1995), Penniston-Dorland and Ferry (2008) and Ague (2011).

elements show variation within the halo which is variably systematic and symmetrical about the midpoint of the halo.

*Chemical variation measured by portable XRF.*—Modeling of fluid flow along the fractures at Delfini required a tracer that is mobile in a metamorphic fluid and that can be reliably measured using the portable XRF analyzer. The portable XRF analyzer was used to take advantage of its higher spatial resolution (sample spacing = 1 – 2 cm compared with 5 cm for conventional XRF analysis). For this purpose and based on findings from conventional XRF analysis, we selected Sr as this tracer. To reduce the effects of heterogeneous mineral modes at the small scale of portable XRF analysis (1 cm), we used the Sr/Ca ratio rather than absolute concentrations of Sr. This works because calcite is the only calcic mineral within the haloes and its mode is approximately constant across each halo. The Sr/Ca ratio decreases towards the fractures in all five profiles (fig. 12). The Sr/Ca ratio is about 0.015 in the country rock. It decreases to ~0.01 in profiles 1 and 2, ~0.005 in profiles 3 and 4 and ~0.002 in profile 5. The Sr/Ca ratios in profile 5 analyzed by the portable XRF are similar to the Sr/Ca ratios measured by conventional XRF (fig. 11). However, spatial resolution of the portable XRF profile is far better and thus more clearly reveals the shape of the Sr/Ca ratio fronts.

## DISCUSSION

### *Effects of Fluid Infiltration*

Fluid flow along the fractures caused a number of changes to the adjacent host rock both mineralogically and chemically.

In the halo, minerals from the country rock such as phengite and omphacite show partial or complete carbonation. The degree of alteration is strongest close to the fracture as is shown by marked decrease in modes of the reactant minerals (fig. 6). Based on variation in calcite mode, we can conclude that the higher volatile content of

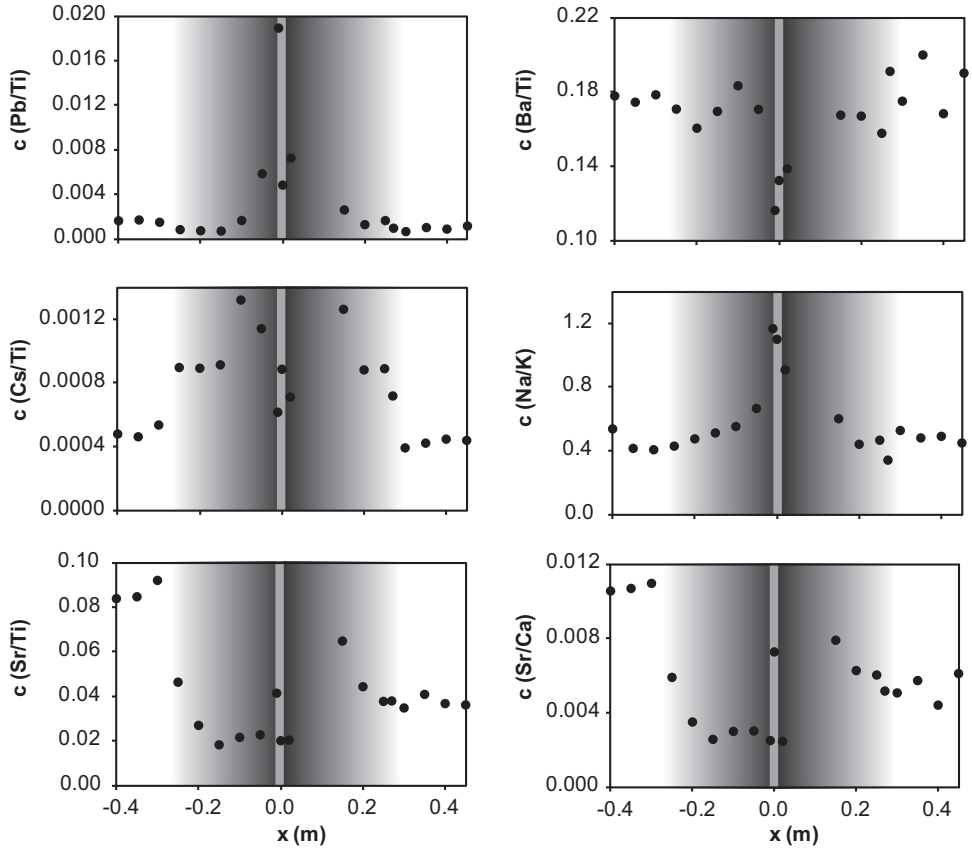


Fig. 11. Variations in trace element ratios along profile 5.

the halo corresponds to a higher concentration of $CO_2$. This is reflected in the breakdown of Ca-bearing mineral phases such as epidote and omphacite (figs. 7B and 8C) to form calcite. With the exception of volatile components ($H_2O$ and $CO_2$) and some mobile elements (Na, K, Cs, Ba, Pb and Sr) carbonation was mostly isochemical and thus had no effect on the LOI-normalized concentrations of most major elements (fig. 9).

A possible generalized carbonation reaction, which consume omphacite, epidote and white mica and produce biotite, chlorite, albite and calcite and might therefore have occurred in the halo, is:

$$5.5\ \text{omphacite} + 10.0\ \text{phengite} + 1.0\ \text{epidote} + 2.4\ Na^+ + 56.5\ H^+ + 4.7\ CO_2 \Rightarrow$$

$$1.0\ \text{biotite} + 5.7\ \text{albite} + 1.0\ \text{chlorite} + 26.0\ \text{quartz} + 4.7\ \text{calcite} + 7.1\ K^+ + 33.8\ H_2O$$

$$5.5\ Ca_{0.5}Na_{0.5}Mg_{0.2}Fe_{0.4}Al_{0.4}Si_{2.0}O_6 + 10.0\ K_{0.8}Al_{1.4}Mg_{0.3}Si_{3.5}Al_{0.5}O_{10}(OH)_2 + 1.0\ Ca_{1.9}Al_{2.0}Fe_{0.9}Si_{3.0}O_{12}(OH) + 2.4\ Na^+ + 56.5\ H^+ + 4.7\ CO_2 \Rightarrow$$

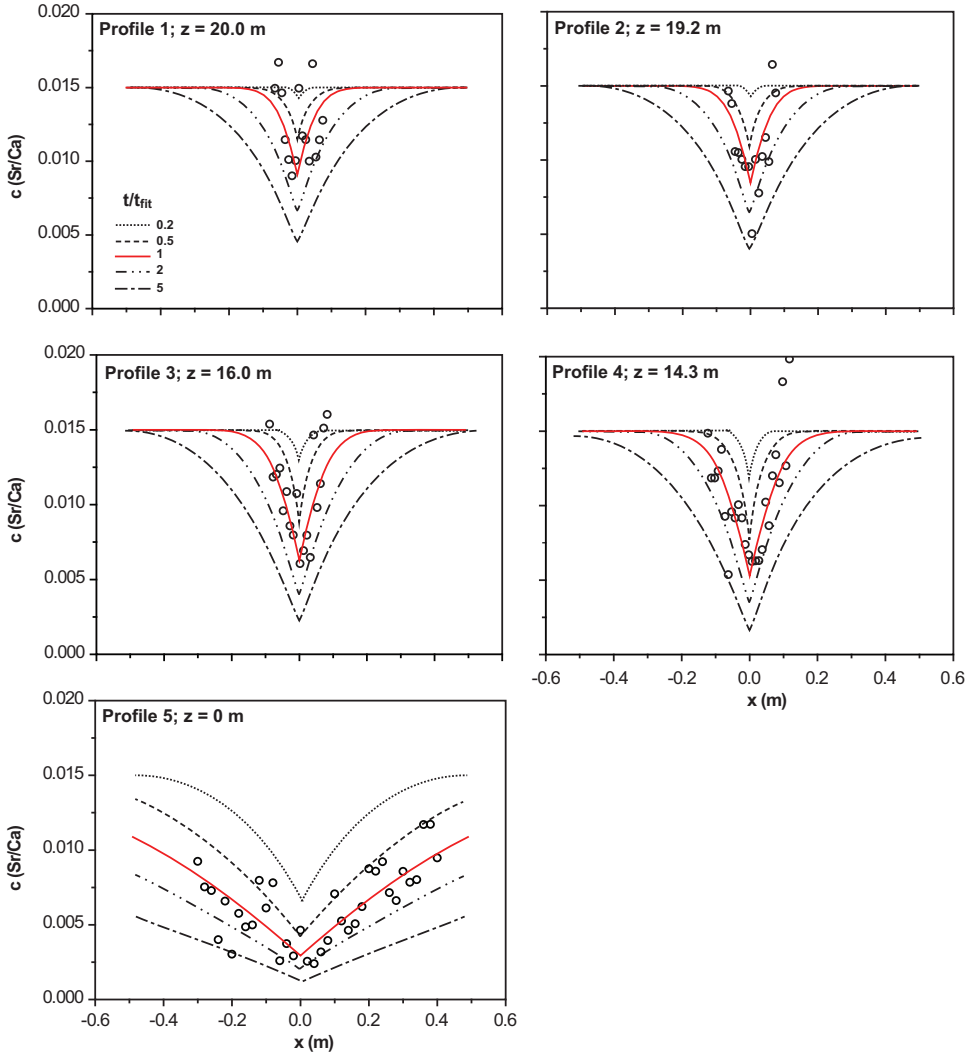


Fig. 12. Sr/Ca ratio across all five profiles with separate best fits for profiles 1–4 and profile 5 (red lines, solid black lines in print version). The $R^2$-value for profiles 1–4 is 0.51 and for profile 5 the $R^2$ value is 0.60. Additional concentration curves for different durations of fluid flow are displayed (dashed lines).

$$1.0\ K_{0.9}Mg_{1.4}Fe_{1.1}Al_{1.2}Si_{3.0}O_{10}(OH)_2 + 1.0\ Mg_{2.7}Fe_{1.9}Al_{2.3}Si_{2.9}O_{10}(OH) + 5.7\ Na_{0.9}Al_{1.0}Si_3O_8 + 26.0\ SiO_2 + 4.7\ CaCO_3 + 7.1\ K^+ + 33.8\ H_2O \quad (r.1)$$

The chemical composition of the minerals involved in r. 1 are taken from table 3. This reaction is supported by textural, modal and chemical data. Whole rock bulk analyses by conventional XRF show that the concentrations of K and Na gradually decrease and increase, respectively, towards the fracture. These elements are more mobile than the other major elements and can be added or removed by a fluid-rock interaction (see review of Jiang and others, 2005). Figure 9 shows that the Na/K ratio

TABLE 5

*(A) Flow velocities, flow durations and diffusion coefficients for a range of values of 2b for profiles 1–4. (B) Flow velocities, flow durations and diffusion coefficients for 2b = 5 mm for profiles 1–4 including a range of values of porosity. (C) Flow velocities, flow durations and diffusion coefficients for 2b = 5 mm for profiles 1–4 including a range of values of $K_v$. (D) Flow velocities, flow durations and diffusion coefficients for a range of values of 2b for profile 5 at different distances along z*

| | fracture aperture 2b, mm | Porosity | Kv | Distance along z, m | Flow velocity log(v), m/s | Duration log(t), year | Diffusion coefficient log(D), $m^2/s$ |
|---|---|---|---|---|---|---|---|
| A | 2 | 0.001 | 0.001 | | -4.72 | 0.31 | -7.15 |
| | 5 | 0.001 | 0.001 | | -5.27 | 0.46 | -7.3 |
| | 10 | 0.001 | 0.001 | | -7.71 | 2.6 | -9.43 |
| B | 5 | 0.01 | 0.001 | | -5.58 | 1.75 | -8.6 |
| | 5 | 0.001 | 0.001 | | -5.27 | 0.46 | -7.3 |
| | 5 | 0.0001 | 0.001 | | -4.98 | -0.68 | -6.04 |
| C | 5 | 0.001 | 0.01 | | -4.82 | -0.84 | -6.89 |
| | 5 | 0.001 | 0.001 | | -5.27 | 0.46 | -7.3 |
| | 5 | 0.001 | 0.0001 | | -5.74 | 1.91 | -7.77 |
| D | 2 | | | 3.36 | -5.94 | 1.88 | -7.15 |
| | 5 | | | 20.61 | -5.7 | 2.03 | -7.3 |
| | 10 | | | 151.98 | -7.27 | 4.16 | -9.43 |

increases towards the fracture which provides evidence of Na-K exchange associated with fluid flow along fractures. This trend is reflected in the replacement of omphacite and white mica by albite (fig. 8D) and replacement of phengite and biotite by chlorite close to the fracture (fig. 7C). This implies that the breakdown of phengite, omphacite and biotite to albite and chlorite close to the fracture was partly metasomatic in character. Earlier studies showed that the metamorphic fluid that caused retrogression was hydrous ($X_{CO2}$ ~0.01; Schumacher and others, 2008b).

We conclude that infiltration of $CO_2$ and $H_2O$ from the fracture into the adjacent country rock caused replacement of Ca-bearing phases by calcite throughout the halo and metasomatic Na-K exchange close to the fracture.

### *Parameterization of Fluid Flow in the Fracture-Halo System*

Five profiles of Sr/Ca were constructed at Delfini (fig. 4). Inverse modeling of these data was performed to constrain fluid flow velocities, flow durations and diffusion coefficients. Best fits of equations (22) and (23) to our data are shown in figure 12 and best fit parameters are listed in table 5. Table 5 shows fluid flow velocities, flow durations and diffusion coefficients calculated for a range of values of $2b$, $\theta$ and $K_\nu$ for Sr. Table 5A considers variation of $2b$. Values were calculated with $K_\nu$ for Sr = $10^{-3}$, $\theta = 10^{-3}$ and $2b = 2$, 5 and 10 mm. This was to span the range of fracture widths seen in the field. Table 5B considers variation of $\theta$. Values were calculated for $K_\nu$ for Sr = $10^{-3}$, 2b = 5 mm and $\theta = 10^{-2}$, $10^{-3}$ and $10^{-4}$. This was to span typical values from the literature (Norton and Knapp, 1977; Connolly, 1997; Skelton, 2011). Table 5C considers variation of $K_\nu$ for Sr. Values were calculated with $2b = 5$ mm, $\theta = 10^{-3}$ and $K_\nu$ for Sr = $10^{-2}$, $10^{-3}$ and $10^{-4}$. This was to span values from the literature. For example Bickle (1992) used a value of $10^{-3}$ based on an assumed concentration of Sr in metamorphic fluid of ~1 ppm. Also, based on a factor of 0.09 for fractionation of Ca and Sr between calcite and fluid (Liebscher and others, 2009), we calculated a value of 0.007 to 0.036 for $K_\nu$ of Sr from our data. Best fits shown in figure 12 were obtained by

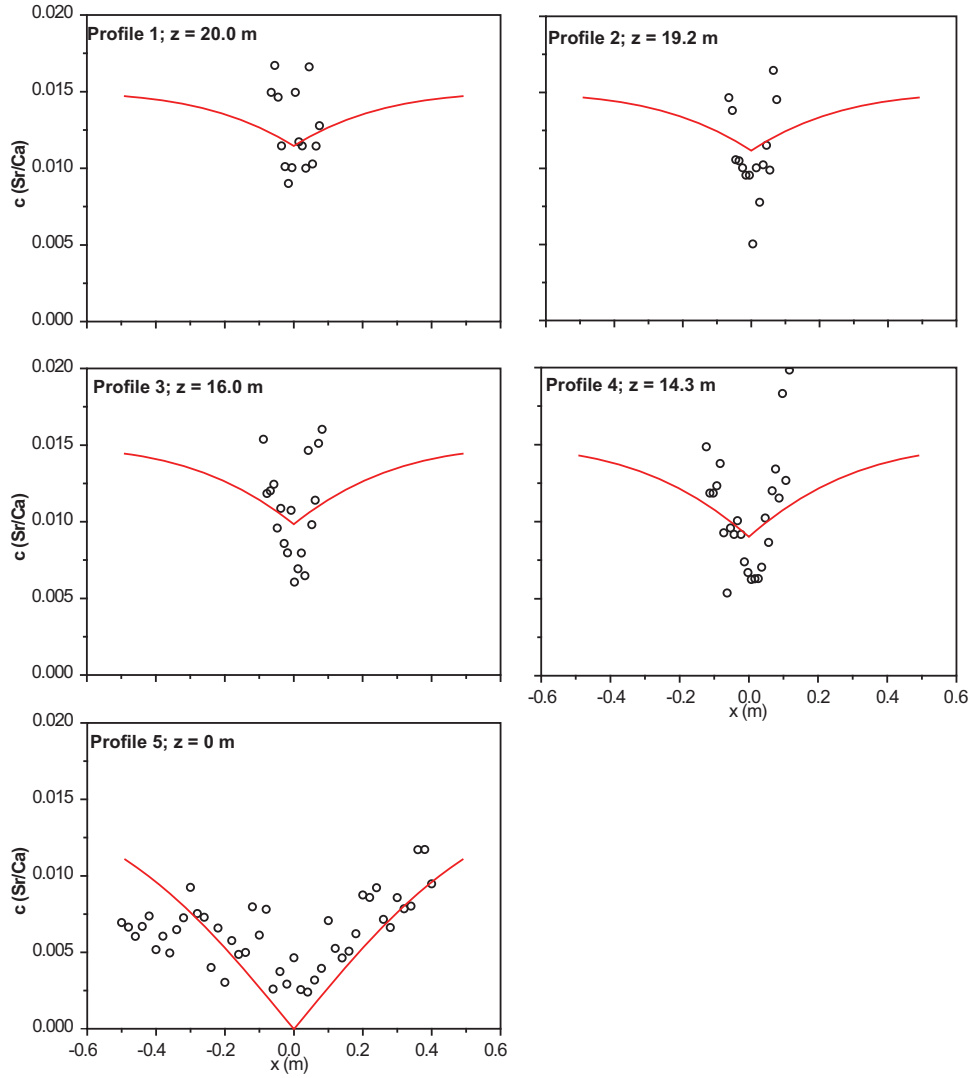


Fig. 13. Sr/Ca ratio across all five profiles were best-fits were obtained including profile 5. Including profile 5 severely reduced goodness-of-fit of the model to our data.

excluding profile 5 and fitting profiles 1 to 4 simultaneously with a common value of $b$ for all four profiles. Their goodness-of-fit, given by the coefficient of multiple determination, is $R^2 = 0.51$. Including profile 5 severely reduced goodness-of-fit of the model to our data (fig. 13). Table 5A shows that larger values of $2b$ gives slower flow velocities and smaller diffusion coefficients, but longer timescales. Note that with $2b = 5$ mm, the best-fit diffusion coefficient is close to the value of $10^{-8}$ $m^2s^{-1}$ which was determined experimentally by Wark and Watson (2004) (table 5A). For this fracture width, flow velocity is 0.005 $mms^{-1}$ or 0.02 $mhr^{-1}$ and flow duration is 2.9 years for $\theta = 10^{-3}$ and $K_\nu$ for Sr $= 10^{-3}$. For $\theta$ ranging from $10^{-2}$ to $10^{-4}$ (table 5B) and $K_\nu$ for Sr ranging from $10^{-2}$ to $10^{-4}$ (table 5C) flow velocities ranges from $10^{-6}$ to $10^{-5}$ $ms^{-1}$ and flow duration ranges from 0.1 to 80 years. This result points to reaction front propagation

caused by rapid fluid flow over a short period of time. In this respect it is of interest to compare the fracture-halo systems described in this study with eclogitized haloes around fractures in Precambrian anorthositic granulites in the Bergen Arcs. These fracture-halo systems which were described by Austrheim (1987) are remarkably similar in appearance, with well-defined sharp reaction fronts, and are of similar widths to the fracture-halo systems at Delfini. Putnis and Austrheim (2010) showed that propagation of these eclogitization fronts was in part by an interface-coupled dissolution/precipitation mechanism. This is important to our study because interface-coupled dissolution/precipitation is a rapid process occurring on the timescales of laboratory experiments (Wood and Walther, 1983; Walther and Wood, 1984; Putnis and Austrheim, 2010) which may explain the rapid reaction front propagation. In making this comparison it is important to note that fracture-halo systems in the Bergen Arcs are hosted by potentially dry granulite facies rocks, whereas fracture-halo systems at Delfini are hosted by greenschist facies rocks which were affected by not only channeled fluid flow along fractures but also pervasive fluid flow in the host rock (Schliestedt and Matthews, 1987). We envisage a scenario similar to that described by Kleine and others (2014) with slower pervasive fluid flow in the country rocks and faster channeled fluid flow along the fractures. In this scenario, competition between these flow regimes sets the width of the haloes.

An interesting finding from the inverse modeling is that the goodness-of-fit was greatly reduced when profile 5 was included (fig. 13). Possible explanations include the following:

1) Profile 5 records overlapping effects of fluid flow along two fractures. This could occur because of a second fracture-halo system which is close to one side of profile 5 (fig. 2). However, goodness-of-fit was only slightly improved by fitting both sides of this profile separately.
2) The fluid composition was different, suggesting that the fracture-halo systems reflect multiple fluid flow events.
3) Measured fracture widths differ from fracture width at the time of fluid flow.
4) A "steady state" was reached at which the rate of diffusive transport of matter to/from the fracture (perpendicular to the fracture) was equal to the rate of advective transport of matter in the country rock (parallel to the fracture).

We favor the fourth explanation, because a steady state is also inferred by the observation of a well-defined maximum halo width of 60 cm at Delfini (fig. 14). Also this type of mechanism was proposed by Kleine and others (2014) to explain preservation of blueschist facies minerals alongside a shear zone at greenschist facies conditions close to the village of Fabrika which is on the southern end of Syros close to Vari (see fig. 1). Fitting profile 5 separately with best-fit diffusion coefficients from profiles 1 to 4 (table 5D) gives a much improved goodness-of-fit $R^2 = 0.60$ but with flow velocities that are *ca.* 2 orders-of-magnitude slower and flow durations that are *ca.* 30 times longer than obtained for profiles 1 to 4 (table 5A). The longer flow duration and/or slower flow velocity are, however, consistent with some longer-lived steady state having been reached. In summary, results from profiles 1 to 4 yield information about flow velocity at the time of fracture propagation and halo widening, whereas profile 5 yields information about steady state flow velocities in the fractures compared with the country rocks.

### *Timing of Fluid Flow*

Fractures within the greenschist facies metamorphosed quartz-mica schists at Delfini are dominantly of extensional, brittle origin and show similarities to the appearance of those calcite-quartz veins described by Famin and others (2004) on Tinos Island. This would point to a later stage of fluid infiltration during uplift and exhumation than reported from the coastline at Fabrika, SE Syros by Kleine and others

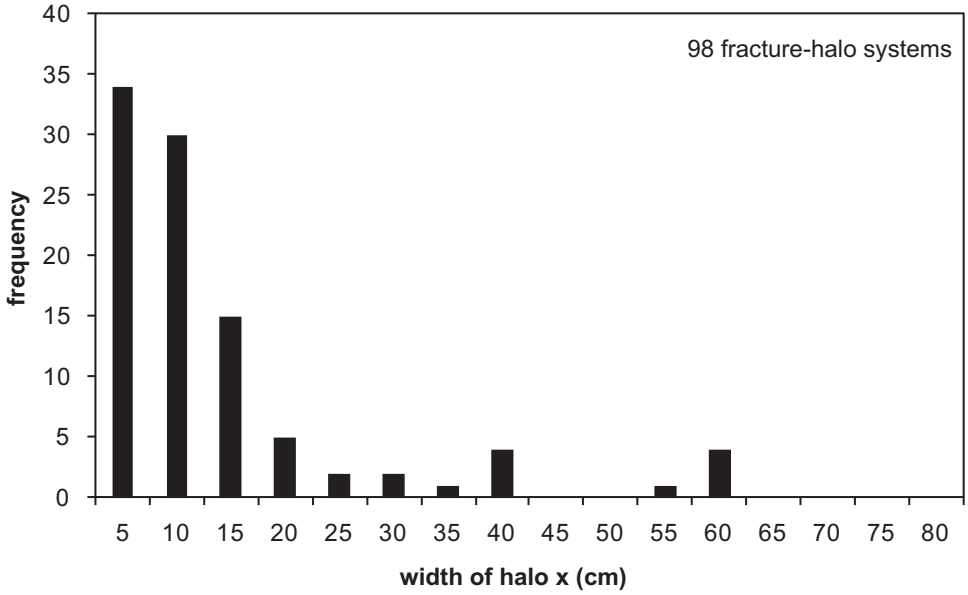


Fig. 14. Distribution of halo widths of 98 fracture-halo systems at Delfini.

(2014). There, the occurrence and preservation of blueschist facies minerals indicate that fluid flow along the studied shear-zone took place at pressure and temperature conditions where HP-LT minerals are still stable. Relicts of omphacite that are most likely derived from higher pressure and temperature regimes are highly altered not only within haloes but also in the host rock in the outcrops at Delfini. High Si-values in phengites could be inherited from HP-facies conditions (Bröcker and others, 1993) but other evidence of the presence of HP-LT minerals could not be found. Further, the $CO_2$-bearing fluid would have been sufficiently fast to preserve potentially present HP-LT minerals as it was described by Kleine and others (2014). However, minerals stable at greenschist facies conditions such as chlorite, biotite and albite were newly formed in the reaction halos during fluid infiltration. This and the brittle habit of the fractures would point to the conclusion that fluid infiltration most likely occurred during a late stage of retrograde greenschist facies metamorphism.

### *Implications for Subduction Zone Metamorphism*

The formation of the haloes surrounding the fractures at Delfini was caused by a hydrous $CO_2$-bearing fluid. Major mass transfer from or into the fractures has not been observed at Delfini. Only relatively mobile elements such as LILEs and Pb show some minor mobility. We speculate that the mobility of these elements was induced by the same fluids that caused leaching of these elements as they passed through the subducting metasedimentary rocks as reported in several other studies (Breeding and others, 2004; Marschall and others, 2006). Periods of fluid flow along the fractures at Delfini were short-lived which may imply that fluid flow in subduction zones occurs episodically as a series of rapid pulses. This is in agreement with other studies of subduction related fluid flow. Penniston-Dorland and others (2010) used small-scale diffusion profiles of Li-isotopes to demonstrate that fluid infiltration events are likely to be much shorter in duration than the overall duration of metamorphism. Further, John and others (2012) used the Li-Ca-Sr isotope systems to constrain the duration of

fluid deriving from a subducting slab. They showed that fluid flow occurred in pulses with durations of about 200 years. These are even shorter than calculated in our study. The brittle character of the fractures at Delfini could point to fluctuating fluid pressure either related to exhumation or to episodic release of volatiles during metamorphic reactions in the subducting slab. In the latter case, the fluids could have used open space such as cracks and fractures of the cooling crust during exhumation as preferred fluid pathways.

## CONCLUSIONS

Late stage fluid flow along fractures within greenschist facies metamorphosed quartz-mica schists at Delfini, NW Syros, was rapid and relatively short-lived. This fluid flowed along conjugate fractures forming carbonated haloes and causing mobility of some major (K and Na) and trace elements (Sr, Cs, Ba, Pb). Inverse modeling of Sr/Ca ratios revealed an early stage of fracture-controlled fluid flow:

- fluid velocities ranged from $10^{-6}$ to $10^{-5}$ $ms^{-1}$
- fluid flow durations lasted from 0.1 to 400 years

for porosities of $10^{-2}$ to $10^{-4}$, volumetric fluid/ solid partition coefficients for Sr of $10^{-2}$ to $10^{-4}$ and fracture widths of 1 to 10 mm. We further suggest that a steady state developed at which halo width was maintained at around 60 cm. Fluid velocities during this state were significantly lower with $10^{-8}$ to $10^{-6}$ $ms^{-1}$ and fluid flow lasted 100 to 15000 years. However, these time-averaged values calculated for a fracture-controlled fluid flow can alternatively record a series of even shorter and faster pulses, perhaps associated with fracture propagation and associated seismicity.

## ACKNOWLEDGMENTS

This work has been financially supported by the EU Initial Training Network DeltaMIN (Mechanisms of Mineral Replacement Reactions) grant, the Bolin Center of Climate Research at Stockholm University, and the Navarino Environmental Observatory (NEO), Messinia, Greece, a cooperation between Stockholm University, the Academy of Athens and TEMES S.A.. XRF and LA-ICP-MS analyses were generated at the lab facilities of the Department of Geological Sciences, Stockholm University, which are partially supported by the Knut & Alice Wallenberg Foundation. The authors would like to thank A. Barker, R. Jacobson, M. Kleine, C. Wohlgemuth-Überwasser and D. Zetterberg for their contribution during sample preparation and analyses. The authors also would like to thank H. Marschall, S. Penniston-Dorland and an anonymous reviewer for their constructive reviews that improved this manuscript.

## Appendix 1

*Chemical data obtained by portable XRF for all five profiles*

| z (cm) | comment | Al | Si | S | Cl | K | Ca | Ti | V | Mn | Fe | Rb | Sr | Zr | LE |
|---|---|---|---|---|---|---|---|---|---|---|---|---|---|---|---|
| | | | | | | | profile 1 | | | | | | | | |
| -6.5 | country rock | 11.89 | 37.99 | n.d. | 1.58 | 7.12 | 2.14 | 0.25 | 0.04 | 0.12 | 4.49 | 0.02 | 0.03 | 0.01 | 35.89 |
| -5.5 | country rock | 11.39 | 35.79 | 0.15 | 0.82 | 4.98 | 5.05 | 0.23 | 0.03 | 0.14 | 4.89 | 0.02 | 0.08 | 0.02 | 37.36 |
| -4.5 | halo | n.d. | 31.51 | 0.18 | 0.91 | 2.94 | 11.91 | 0.18 | 0.02 | 0.13 | 3.59 | 0.01 | 0.17 | 0.03 | 49.48 |
| -3.5 | halo | 9.18 | 37.22 | 0.26 | 1.00 | 4.96 | 7.67 | 0.19 | 0.03 | 0.14 | 4.02 | 0.02 | 0.09 | 0.01 | 36.46 |
| -2.5 | halo | 7.20 | 41.78 | 0.24 | 0.83 | 4.86 | 6.02 | 0.25 | 0.03 | 0.13 | 4.10 | 0.02 | 0.06 | 0.01 | 35.54 |
| -1.5 | halo | 10.39 | 36.13 | 0.37 | 0.90 | 4.75 | 6.22 | 0.22 | 0.04 | 0.16 | 4.89 | 0.02 | 0.06 | 0.02 | 37.07 |
| -0.5 | halo | 7.02 | 32.10 | 0.28 | 0.76 | 4.05 | 6.53 | 0.33 | 0.03 | 0.18 | 5.28 | 0.02 | 0.07 | 0.02 | 44.34 |
| 0.5 | halo | 9.32 | 33.30 | 0.54 | 0.89 | 3.99 | 6.88 | 0.25 | 0.03 | 0.15 | 4.74 | 0.02 | 0.10 | 0.01 | 41.19 |
| 1.5 | halo | 9.02 | 34.41 | n.d. | 0.60 | 4.40 | 7.08 | 0.27 | 0.10 | 0.16 | 4.64 | 0.02 | 0.08 | 0.01 | 39.73 |
| 2.5 | halo | 6.58 | 34.03 | 0.25 | 0.72 | 4.64 | 5.40 | 0.31 | 0.03 | 0.17 | 5.50 | 0.02 | 0.06 | 0.01 | 43.24 |
| 3.5 | halo | 10.61 | 35.26 | 0.40 | 0.99 | 6.33 | 2.65 | 0.25 | 0.05 | 0.15 | 5.13 | 0.02 | 0.03 | 0.01 | 39.50 |
| 4.5 | halo | 9.82 | 31.48 | 0.27 | 0.85 | 5.71 | 4.16 | 0.26 | 0.05 | 0.20 | 6.58 | 0.02 | 0.07 | 0.02 | 41.04 |
| 5.5 | halo | 10.85 | 38.13 | 0.55 | 0.65 | 5.15 | 4.45 | 0.46 | 0.04 | 0.20 | 6.51 | 0.02 | 0.05 | 0.02 | 33.42 |
| 6.5 | country rock | 11.93 | 40.58 | 0.61 | 0.70 | 4.84 | 3.75 | 0.31 | 0.04 | 0.19 | 6.14 | 0.02 | 0.04 | 0.01 | 32.12 |
| 7.5 | country rock | 10.42 | 38.87 | 0.12 | 0.54 | 5.45 | 4.28 | 0.29 | 0.04 | 0.17 | 5.43 | 0.02 | 0.05 | 0.01 | 34.96 |
| | | | | | | | profile 2 | | | | | | | | |
| -6.5 | country rock | 13.31 | 29.95 | 0.18 | 0.72 | 6.51 | 3.03 | 0.46 | 0.05 | 0.16 | 6.03 | 0.03 | 0.04 | 0.02 | 40.38 |
| -5.5 | country rock | 12.27 | 35.14 | 0.19 | 0.76 | 6.11 | 3.12 | 0.33 | 0.04 | 0.18 | 6.30 | 0.02 | 0.04 | 0.02 | 36.40 |
| -4.5 | halo | 12.87 | 33.51 | 0.14 | 0.85 | 5.52 | 2.87 | 0.34 | 0.04 | 0.16 | 5.40 | 0.02 | 0.03 | 0.02 | 39.19 |
| -3.5 | halo | 12.75 | 30.91 | 0.13 | 1.27 | 6.76 | 3.09 | 0.36 | 0.05 | 0.19 | 6.63 | 0.03 | 0.03 | 0.02 | 39.15 |
| -2.5 | halo | 11.15 | 32.99 | 0.29 | 0.82 | 5.62 | 3.42 | 0.28 | 0.05 | 0.18 | 6.07 | 0.02 | 0.03 | 0.02 | 40.14 |
| -1.5 | halo | 11.47 | 32.34 | 0.61 | 0.63 | 6.17 | 3.20 | 0.34 | 0.05 | 0.17 | 6.08 | 0.02 | 0.03 | 0.03 | 40.08 |
| -0.5 | halo | 10.27 | 31.81 | 0.68 | 1.97 | 3.16 | 4.29 | 0.34 | 0.03 | 0.12 | 5.45 | 0.01 | 0.04 | 0.03 | 44.42 |
| 0.5 | halo | 11.58 | 32.54 | 0.51 | 1.63 | 4.00 | 10.24 | 0.39 | 0.04 | 0.18 | 4.62 | 0.02 | 0.05 | 0.02 | 36.30 |
| 1.5 | halo | 13.24 | 33.35 | 0.36 | 6.95 | 5.15 | 3.23 | 0.32 | 0.04 | 0.15 | 5.69 | 0.02 | 0.03 | 0.02 | 38.75 |
| 2.5 | halo | 7.94 | 38.05 | 0.27 | 2.22 | 5.31 | 2.92 | 0.25 | 0.04 | 0.17 | 5.63 | 0.02 | 0.02 | 0.02 | 39.61 |
| 3.5 | halo | 10.63 | 37.59 | 0.33 | 2.04 | 4.56 | 4.16 | 0.23 | 0.03 | 0.15 | 4.82 | 0.02 | 0.04 | 0.03 | 37.70 |
| 4.5 | halo | 12.34 | 34.84 | 0.44 | 1.56 | 5.45 | 5.58 | 0.32 | 0.04 | 0.19 | 5.15 | 0.02 | 0.06 | 0.02 | 35.98 |
| 5.5 | halo | 12.93 | 36.45 | 0.47 | 1.87 | 4.65 | 4.39 | 0.23 | 0.03 | 0.18 | 6.02 | 0.02 | 0.04 | 0.02 | 35.01 |
| 6.5 | country rock | 15.14 | 35.32 | 0.27 | 2.19 | 5.06 | 4.01 | 0.25 | 0.04 | 0.15 | 5.26 | 0.02 | 0.07 | 0.02 | 34.64 |
| 7.5 | country rock | 7.78 | 35.28 | 0.52 | 0.83 | 3.93 | 9.70 | 0.20 | 0.03 | 0.17 | 4.77 | 0.02 | 0.14 | 0.02 | 37.97 |
| | | | | | | | profile 3 | | | | | | | | |
| -8.75 | country rock | 7.89 | 36.17 | 0.33 | 1.03 | 4.96 | 4.96 | 0.21 | 0.04 | 0.17 | 4.42 | 0.02 | 0.08 | 0.02 | 41.06 |
| -7.75 | country rock | 10.01 | 32.66 | 0.25 | 1.23 | 4.07 | 7.41 | 0.19 | 0.03 | 0.16 | 4.94 | 0.02 | 0.09 | 0.01 | 40.40 |
| -6.75 | halo | 12.01 | 35.85 | 0.49 | 0.65 | 4.91 | 4.93 | 0.22 | 0.04 | 0.18 | 5.98 | 0.02 | 0.06 | 0.02 | 35.75 |
| -5.75 | halo | 10.26 | 34.51 | 0.33 | 0.97 | 5.14 | 4.53 | 0.23 | 0.04 | 0.16 | 5.55 | 0.02 | 0.06 | 0.01 | 39.48 |
| -4.75 | halo | 9.53 | 32.05 | 0.23 | 3.96 | 5.31 | 4.11 | 0.31 | 0.04 | 0.14 | 5.21 | 0.02 | 0.04 | 0.02 | 43.19 |
| -3.75 | halo | n.d. | 26.34 | 0.37 | 0.70 | 3.69 | 5.48 | 0.22 | 0.02 | 0.12 | 4.31 | 0.02 | 0.06 | 0.01 | 59.69 |
| -2.75 | halo | 7.83 | 33.89 | 1.21 | n.d. | 3.40 | 7.86 | 0.23 | 0.03 | 0.14 | 4.50 | 0.02 | 0.07 | 0.02 | 41.97 |
| -1.75 | halo | 9.78 | 34.23 | 0.69 | n.d. | 3.85 | 5.94 | 0.21 | 0.03 | 0.15 | 5.00 | 0.02 | 0.05 | 0.03 | 40.70 |
| -0.75 | halo | 12.11 | 34.68 | 0.25 | n.d. | 4.36 | 5.22 | 0.26 | 0.03 | 0.14 | 5.55 | 0.02 | 0.06 | 0.02 | 37.54 |
| 0.25 | halo | 6.79 | 36.55 | 0.32 | n.d. | 3.65 | 5.96 | 0.32 | 0.03 | 0.12 | 4.29 | 0.02 | 0.04 | 0.02 | 42.18 |
| 1.25 | halo | 11.16 | 34.03 | 0.00 | n.d. | 3.82 | 5.53 | 0.38 | 0.03 | 0.12 | 4.58 | 0.02 | 0.04 | 0.01 | 39.46 |
| 2.25 | halo | 11.57 | 30.71 | 0.20 | n.d. | 4.41 | 5.11 | 0.28 | 0.03 | 0.16 | 5.40 | 0.02 | 0.04 | 0.01 | 42.23 |
| 3.25 | halo | 12.58 | 29.12 | 0.14 | n.d. | 4.13 | 6.42 | 0.41 | 0.03 | 0.16 | 4.67 | 0.02 | 0.04 | 0.02 | 42.39 |
| 4.25 | halo | 9.37 | 30.99 | 0.23 | 1.59 | 5.59 | 3.20 | 0.32 | 0.06 | 0.14 | 5.55 | 0.02 | 0.05 | 0.02 | 44.65 |
| 5.25 | halo | 9.13 | 31.34 | 0.29 | 1.54 | 4.59 | 3.78 | 0.31 | 0.05 | 0.12 | 4.87 | 0.02 | 0.04 | 0.03 | 45.70 |
| 6.25 | country rock | 7.90 | 29.92 | 0.31 | 1.67 | 5.79 | 4.98 | 0.32 | 0.05 | 0.14 | 6.25 | 0.02 | 0.06 | 0.02 | 44.55 |
| 7.25 | country rock | 11.26 | 31.70 | 0.22 | 0.67 | 5.11 | 4.09 | 0.37 | 0.04 | 0.13 | 5.71 | 0.02 | 0.06 | 0.01 | 41.48 |
| 8.25 | country rock | 7.51 | 33.82 | 0.33 | 1.63 | 4.52 | 6.66 | 0.38 | 0.04 | 0.13 | 5.27 | 0.02 | 0.11 | 0.01 | 41.52 |
| | | | | | | | profile 4 | | | | | | | | |
| -12.25 | country rock | 6.94 | 32.87 | 0.14 | 2.58 | 4.69 | 6.77 | 0.45 | 0.03 | 0.12 | 5.44 | 0.02 | 0.10 | 0.01 | 41.97 |
| -11.25 | country rock | 8.42 | 37.40 | 0.27 | 2.04 | 4.14 | 5.45 | 0.38 | 0.03 | 0.09 | 4.27 | 0.02 | 0.06 | 0.02 | 39.70 |
| -10.25 | country rock | 7.91 | 38.08 | 0.36 | 1.67 | 2.90 | 8.07 | 0.26 | 0.02 | 0.10 | 3.65 | 0.01 | 0.10 | 0.01 | 38.87 |
| -9.25 | country rock | 7.59 | 38.58 | 0.31 | 1.71 | 2.77 | 5.75 | 0.26 | 0.02 | 0.09 | 3.74 | 0.01 | 0.07 | 0.01 | 41.10 |
| -8.25 | country rock | n.d. | 32.34 | 0.41 | 9.60 | 3.56 | 4.94 | 0.21 | 0.02 | 0.10 | 3.37 | 0.02 | 0.07 | 0.01 | 55.35 |
| -7.25 | halo | 10.44 | 32.12 | 0.89 | 2.93 | 5.43 | 5.00 | 0.28 | 0.03 | 0.13 | 5.51 | 0.02 | 0.05 | 0.02 | 40.94 |
| -6.25 | halo | 8.30 | 30.34 | 0.76 | 0.82 | 3.67 | 11.99 | 0.28 | 0.03 | 0.16 | 3.85 | 0.02 | 0.06 | 0.02 | 41.25 |
| -5.25 | halo | 5.90 | 35.79 | 0.47 | 0.55 | 3.61 | 7.64 | 0.22 | 0.03 | 0.12 | 3.78 | 0.02 | 0.07 | 0.02 | 42.80 |
| -4.25 | halo | 8.83 | 37.83 | 0.37 | 0.57 | 2.29 | 8.16 | 0.16 | 0.02 | 0.09 | 3.13 | 0.01 | 0.07 | 0.02 | 39.40 |
| -3.25 | halo | 6.28 | 39.34 | 0.52 | 0.85 | 2.34 | 5.86 | 0.22 | 0.02 | 0.08 | 3.43 | 0.01 | 0.06 | 0.01 | 42.33 |
| -2.25 | halo | 7.84 | 39.42 | 0.54 | 1.30 | 3.03 | 4.39 | 0.33 | 0.02 | 0.09 | 4.26 | 0.01 | 0.04 | 0.01 | 40.55 |
| -1.25 | halo | 11.50 | 39.10 | 0.45 | 1.54 | 3.13 | 3.97 | 0.38 | 0.02 | 0.09 | 4.82 | 0.01 | 0.03 | 0.02 | 36.90 |
| -0.25 | halo | 13.61 | 34.12 | 0.19 | 2.33 | 3.83 | 4.54 | 0.49 | 0.04 | 0.12 | 4.87 | 0.02 | 0.03 | 0.03 | 38.28 |
| 0.75 | halo | 12.63 | 33.31 | 0.28 | 0.63 | 4.42 | 4.66 | 0.37 | 0.03 | 0.11 | 5.11 | 0.02 | 0.03 | 0.02 | 39.25 |
| 1.75 | halo | 12.73 | 33.44 | 0.40 | 1.27 | 4.67 | 5.08 | 0.31 | 0.04 | 0.12 | 4.23 | 0.02 | 0.03 | 0.02 | 39.27 |
| 2.75 | halo | 9.99 | 31.77 | 0.59 | 1.29 | 5.12 | 4.34 | 0.35 | 0.03 | 0.15 | 4.75 | 0.02 | 0.03 | 0.02 | 43.41 |
| 3.75 | halo | 13.87 | 33.01 | 0.48 | 1.03 | 5.52 | 4.15 | 0.35 | 0.05 | 0.18 | 6.55 | 0.03 | 0.03 | 0.02 | 36.21 |
| 4.75 | halo | 9.91 | 38.37 | 0.38 | 0.93 | 4.33 | 4.56 | 0.26 | 0.04 | 0.12 | 4.44 | 0.02 | 0.05 | 0.03 | 37.86 |
| 5.75 | halo | 10.16 | 34.59 | 0.27 | 1.19 | 4.02 | 4.12 | 0.34 | 0.03 | 0.13 | 4.95 | 0.02 | 0.04 | 0.02 | 40.98 |
| 6.75 | halo | n.d. | 26.47 | 0.15 | 5.34 | 4.34 | 4.03 | 0.29 | 0.03 | 0.15 | 5.23 | 0.02 | 0.05 | 0.02 | 59.34 |
| 7.75 | halo | n.d. | 25.69 | 0.16 | 2.51 | 4.33 | 3.60 | 0.28 | 0.02 | 0.12 | 4.33 | 0.02 | 0.05 | 0.01 | 61.52 |
| 8.75 | halo | 11.53 | 36.16 | 0.27 | 0.99 | 4.17 | 3.05 | 0.25 | 0.03 | 0.09 | 5.10 | 0.02 | 0.04 | 0.02 | 39.53 |
| 9.75 | halo | n.d. | 40.52 | 0.48 | 0.82 | 2.11 | 6.13 | 0.17 | 0.02 | 0.07 | 2.64 | 0.01 | 0.11 | 0.01 | 48.20 |
| 10.75 | country rock | 5.15 | 43.56 | 0.62 | 2.48 | 2.92 | 5.23 | 0.14 | 0.02 | 0.08 | 3.28 | 0.01 | 0.07 | 0.01 | 39.52 |
| 11.75 | country rock | 5.58 | 40.80 | 0.68 | 5.34 | 4.07 | 5.02 | 0.22 | 0.04 | 0.22 | 4.23 | 0.01 | 0.10 | 0.02 | 39.66 |

## Appendix 1
*(continued)*

| z (cm) | comment | Al | Si | S | Cl | K | Ca | Ti | V | Mn | Fe | Rb | Sr | Zr | LE |
|---|---|---|---|---|---|---|---|---|---|---|---|---|---|---|---|
| | | | | | | | profile 5 (field) | | | | | | | | |
| -50 | country rock | 8.69 | 29.79 | 1.41 | 13.30 | 5.75 | 5.86 | 0.36 | 0.05 | 0.13 | 6.59 | 0.02 | 0.04 | 0.01 | 42.70 |
| -48 | country rock | n.d. | 37.46 | 1.24 | 7.08 | 3.08 | 12.96 | 0.28 | 0.02 | 0.12 | 4.16 | 0.01 | 0.09 | 0.01 | 41.80 |
| -46 | country rock | 11.70 | 35.15 | 1.02 | 10.82 | 4.87 | 5.29 | 0.45 | 0.04 | 0.11 | 5.95 | 0.02 | 0.03 | 0.02 | 36.35 |
| -44 | country rock | 7.87 | 35.62 | 0.92 | 5.13 | 4.70 | 4.45 | 0.35 | 0.04 | 0.09 | 4.89 | 0.02 | 0.03 | 0.02 | 41.92 |
| -42 | country rock | n.d. | 25.56 | 0.88 | 5.12 | 3.74 | 4.68 | 0.33 | 0.03 | 0.09 | 4.58 | 0.02 | 0.03 | 0.01 | 60.93 |
| -40 | country rock | n.d. | 25.36 | 0.25 | 5.77 | 4.34 | 4.01 | 0.23 | 0.04 | 0.09 | 5.29 | 0.02 | 0.02 | 0.03 | 60.57 |
| -38 | country rock | 10.45 | 27.40 | 0.34 | 17.31 | 5.59 | 4.16 | 0.54 | 0.04 | 0.10 | 6.51 | 0.02 | 0.03 | 0.01 | 45.14 |
| -36 | country rock | n.d. | 35.33 | 0.26 | 33.27 | 7.56 | 7.85 | 0.62 | 0.07 | 0.17 | 8.13 | 0.04 | 0.04 | 0.03 | 40.14 |
| -34 | country rock | 9.59 | 27.49 | 0.37 | 27.08 | 5.70 | 5.55 | 0.51 | 0.04 | 0.10 | 7.73 | 0.03 | 0.04 | 0.04 | 43.17 |
| -32 | country rock | n.d. | 34.39 | 0.54 | 20.04 | 4.04 | 8.30 | 0.31 | 0.03 | 0.09 | 4.18 | 0.02 | 0.06 | 0.02 | 48.55 |
| -30 | halo | 6.16 | 40.66 | 0.49 | 5.72 | 4.64 | 3.60 | 0.31 | 0.03 | 0.07 | 4.44 | 0.02 | 0.03 | 0.01 | 40.03 |
| -28 | halo | 7.15 | 36.80 | 0.34 | 3.77 | 3.08 | 6.49 | 0.35 | 0.02 | 0.07 | 3.98 | 0.01 | 0.05 | 0.01 | 41.99 |
| -26 | halo | 6.15 | 41.36 | 0.54 | 3.83 | 3.47 | 5.42 | 0.29 | 0.02 | 0.08 | 4.49 | 0.01 | 0.04 | 0.01 | 38.65 |
| -24 | halo | 11.43 | 38.08 | 0.61 | 5.62 | 5.02 | 3.32 | 0.26 | 0.04 | 0.09 | 5.27 | 0.02 | 0.01 | 0.02 | 36.44 |
| -22 | halo | n.d. | 35.85 | 0.40 | 3.51 | 3.88 | 5.21 | 0.34 | 0.03 | 0.09 | 3.69 | 0.02 | 0.03 | 0.01 | 50.84 |
| -20 | halo | 9.54 | 29.24 | 0.42 | 3.85 | 4.53 | 4.27 | 0.38 | 0.04 | 0.09 | 4.67 | 0.02 | 0.01 | 0.02 | 47.18 |
| -18 | halo | 13.32 | 33.54 | 0.46 | 2.59 | 5.11 | 5.51 | 0.32 | 0.04 | 0.10 | 4.84 | 0.02 | 0.03 | 0.01 | 37.14 |
| -16 | halo | 7.17 | 41.34 | 0.32 | 2.37 | 3.12 | 5.80 | 0.70 | 0.03 | 0.10 | 4.19 | 0.01 | 0.03 | 0.02 | 37.47 |
| -14 | halo | 9.03 | 36.14 | 0.31 | 2.86 | 2.86 | 6.02 | 0.32 | 0.02 | 0.04 | 4.07 | 0.01 | 0.03 | 0.01 | 41.44 |
| -12 | halo | 6.69 | 41.63 | 0.49 | 3.06 | 2.53 | 6.22 | 0.51 | 0.03 | 0.09 | 3.04 | 0.01 | 0.05 | 0.01 | 39.18 |
| -10 | halo | 9.04 | 33.38 | 0.51 | 2.29 | 2.32 | 6.25 | 0.40 | 0.03 | 0.07 | 4.49 | 0.01 | 0.04 | 0.02 | 43.96 |
| -8 | halo | 7.50 | 40.28 | 0.36 | 6.04 | 2.75 | 8.97 | 0.31 | 0.03 | 0.10 | 2.78 | 0.01 | 0.07 | 0.01 | 37.20 |
| -6 | halo | 10.81 | 32.69 | 0.31 | 2.82 | 4.13 | 5.58 | 0.49 | 0.03 | 0.07 | 5.86 | 0.02 | 0.01 | 0.02 | 40.26 |
| -4 | halo | 10.80 | 32.74 | 0.92 | 7.84 | 2.65 | 8.22 | 0.68 | n.d. | 0.11 | 5.57 | 0.01 | 0.03 | 0.02 | 39.16 |
| -2 | halo | 9.59 | 29.66 | 1.72 | 13.85 | 4.46 | 6.03 | 0.52 | 0.05 | 0.10 | 5.44 | 0.02 | 0.02 | 0.02 | 44.08 |
| 0 | halo | 11.51 | 33.03 | 0.16 | 23.30 | 0.25 | 4.75 | 0.06 | n.d. | 0.04 | 0.88 | 0.00 | 0.02 | 0.00 | 49.44 |
| 2 | halo | 8.00 | 30.73 | 0.52 | 13.49 | 3.98 | 4.92 | 0.46 | 0.04 | 0.11 | 4.94 | 0.02 | 0.01 | 0.02 | 46.75 |
| 4 | halo | n.d. | 28.80 | 0.36 | 22.02 | 5.66 | 6.07 | 0.61 | 0.05 | 0.13 | 6.05 | 0.02 | 0.01 | 0.03 | 52.52 |
| 6 | halo | 13.25 | 28.04 | 0.47 | 5.75 | 5.22 | 4.38 | 0.59 | 0.05 | 0.14 | 5.41 | 0.02 | 0.01 | 0.02 | 42.84 |
| 8 | halo | n.d. | 24.25 | 0.76 | 4.18 | 4.41 | 5.09 | 0.25 | 0.05 | 0.13 | 4.56 | 0.02 | 0.02 | 0.01 | 61.19 |
| 10 | halo | 8.71 | 42.10 | 0.44 | 2.23 | 4.16 | 1.84 | 0.31 | 0.03 | 0.08 | 4.44 | 0.02 | 0.01 | 0.01 | 38.24 |
| 12 | halo | 10.94 | 31.69 | 0.61 | 3.27 | 4.81 | 2.75 | 0.43 | 0.04 | 0.12 | 7.23 | 0.02 | 0.01 | 0.02 | 41.94 |
| 14 | halo | 10.85 | 36.96 | 0.98 | 2.88 | 5.32 | 2.99 | 0.44 | 0.03 | 0.11 | 4.94 | 0.02 | 0.01 | 0.02 | 38.30 |
| 16 | halo | 12.03 | 32.25 | 0.75 | 2.48 | 5.52 | 3.31 | 0.50 | 0.04 | 0.11 | 6.47 | 0.02 | 0.02 | 0.02 | 39.69 |
| 18 | halo | 12.81 | 28.88 | 0.70 | 2.68 | 5.61 | 3.20 | 0.46 | 0.05 | 0.11 | 5.83 | 0.02 | 0.02 | 0.02 | 42.96 |
| 20 | halo | 7.52 | 37.94 | 0.60 | 5.56 | 5.14 | 3.26 | 0.33 | 0.04 | 0.10 | 4.20 | 0.02 | 0.03 | 0.01 | 41.42 |
| 22 | halo | n.d. | 65.39 | 0.43 | 3.07 | 2.09 | 3.93 | 0.08 | 0.01 | 0.05 | 1.38 | 0.01 | 0.03 | 0.00 | 27.02 |
| 24 | halo | 7.32 | 29.54 | 0.46 | 11.86 | 4.37 | 6.54 | 0.21 | 0.03 | 0.11 | 4.68 | 0.02 | 0.06 | 0.02 | 47.09 |
| 26 | halo | 11.62 | 26.88 | 0.61 | 10.93 | 7.61 | 4.43 | 0.46 | 0.07 | 0.16 | 7.19 | 0.03 | 0.03 | 0.02 | 41.47 |
| 28 | halo | 12.08 | 35.96 | 0.83 | 7.30 | 6.21 | 3.19 | 0.27 | 0.05 | 0.13 | 5.47 | 0.02 | 0.02 | 0.02 | 36.58 |
| 30 | country rock | 10.37 | 35.39 | 0.85 | 1.83 | 4.19 | 5.46 | 0.44 | 0.04 | 0.15 | 5.84 | 0.02 | 0.05 | 0.03 | 38.00 |
| 32 | country rock | 15.19 | 33.25 | 0.50 | 6.37 | 6.75 | 3.39 | 0.28 | 0.05 | 0.16 | 6.55 | 0.03 | 0.03 | 0.03 | 34.27 |
| 34 | country rock | 10.87 | 35.56 | 0.82 | 3.95 | 5.63 | 3.64 | 0.25 | 0.03 | 0.15 | 5.52 | 0.02 | 0.03 | 0.02 | 38.26 |
| 36 | country rock | 12.81 | 34.96 | 1.04 | 0.95 | 5.30 | 4.82 | 0.35 | 0.05 | 0.20 | 6.89 | 0.02 | 0.06 | 0.02 | 34.50 |
| 38 | country rock | 15.66 | 34.11 | 0.43 | 0.55 | 6.10 | 3.23 | 0.28 | 0.05 | 0.17 | 5.74 | 0.02 | 0.04 | 0.02 | 34.54 |
| 40 | country rock | 8.07 | 35.59 | 0.30 | 0.75 | 3.95 | 4.72 | 0.21 | 0.03 | 0.13 | 4.07 | 0.02 | 0.04 | 0.02 | 43.14 |
| | | | | | | | profile 5(rock chips) | | | | | | | | |
| -0.4 | country rock | 13.81 | 38.67 | n.d. | n.d. | 5.64 | 3.44 | 0.31 | 0.04 | 0.08 | 5.61 | 0.02 | 0.01 | 0.01 | 32.34 |
| -0.35 | country rock | 14.04 | 36.71 | n.d. | n.d. | 5.44 | 5.26 | 0.34 | 0.05 | 0.07 | 5.70 | 0.02 | 0.03 | 0.03 | 32.29 |
| -0.3 | country rock | 11.39 | 38.86 | n.d. | n.d. | 4.66 | 4.91 | 0.31 | 0.03 | 0.05 | 4.81 | 0.02 | 0.04 | 0.02 | 34.89 |
| -0.25 | halo | 11.03 | 39.31 | n.d. | 0.90 | 5.39 | 4.53 | 0.36 | 0.04 | 0.07 | 5.70 | 0.02 | 0.01 | 0.02 | 33.52 |
| -0.2 | halo | 13.40 | 37.84 | n.d. | 0.14 | 5.56 | 3.91 | 0.29 | 0.03 | 0.07 | 5.32 | 0.02 | 0.01 | 0.01 | 33.52 |
| -0.15 | halo | 9.22 | 41.79 | n.d. | 0.12 | 4.01 | 4.91 | 0.29 | 0.02 | 0.05 | 4.20 | 0.02 | 0.02 | 0.01 | 35.44 |
| -0.1 | halo | 11.92 | 37.64 | n.d. | n.d. | 5.11 | 4.68 | 0.45 | 0.03 | 0.06 | 5.47 | 0.02 | 0.01 | 0.02 | 34.58 |
| -0.05 | halo | 11.94 | 41.48 | n.d. | 0.37 | 4.45 | 4.26 | 0.41 | 0.03 | 0.10 | 4.74 | 0.02 | 0.01 | 0.01 | 32.52 |
| -0.01 | halo | 12.21 | 35.05 | n.d. | 6.63 | 2.65 | 5.61 | 0.47 | 0.03 | 0.08 | 5.67 | 0.01 | 0.01 | 0.02 | 38.14 |
| 0 | halo | 13.50 | 39.06 | n.d. | n.d. | 5.43 | 0.59 | 0.56 | 0.04 | 0.08 | 5.91 | 0.02 | 0.01 | 0.03 | 34.43 |
| 0.1 | halo | 12.00 | 37.17 | n.d. | 2.56 | 4.81 | 7.54 | 0.38 | 0.03 | 0.09 | 5.09 | 0.02 | 0.06 | 0.03 | 32.76 |
| 0.15 | halo | 14.04 | 38.77 | n.d. | 1.13 | 4.61 | 4.59 | 0.36 | 0.03 | 0.06 | 5.26 | 0.02 | 0.01 | 0.02 | 32.22 |
| 0.2 | halo | 12.16 | 42.53 | n.d. | n.d. | 5.17 | 3.85 | 0.29 | 0.04 | 0.10 | 4.39 | 0.02 | 0.01 | 0.01 | 31.43 |
| 0.25 | halo | 13.53 | 39.16 | n.d. | 2.64 | 4.75 | 4.33 | 0.36 | 0.03 | 0.09 | 5.01 | 0.02 | 0.02 | 0.02 | 32.67 |
| 0.3 | halo | 14.83 | 39.37 | n.d. | 12.31 | 5.92 | 3.36 | 0.43 | 0.04 | 0.11 | 6.24 | 0.02 | 0.01 | 0.02 | 29.62 |
| 0.27 | country rock | 11.95 | 39.71 | n.d. | 1.46 | 5.18 | 4.46 | 0.35 | 0.05 | 0.09 | 5.29 | 0.02 | 0.02 | 0.02 | 32.84 |
| 0.35 | country rock | 10.68 | 41.80 | n.d. | n.d. | 4.77 | 3.05 | 0.30 | 0.03 | 0.08 | 5.26 | 0.02 | 0.01 | 0.02 | 33.53 |
| 0.4 | country rock | 11.95 | 41.90 | n.d. | n.d. | 4.44 | 5.61 | 0.22 | 0.03 | 0.07 | 5.19 | 0.02 | 0.04 | 0.02 | 30.52 |
| 0.45 | country rock | 12.44 | 42.01 | n.d. | 1.70 | 6.01 | 3.72 | 0.34 | 0.04 | 0.08 | 5.66 | 0.02 | 0.01 | 0.02 | 29.63 |

Chemical data obtained by portable XRF for all five profiles. LE = light elements (elements lighter than Mg). The influence of sea salt (NaCl and $Na_2SO_4$) was removed from the measurements and the data values were recalculated accordingly. All values are shown in wt.%. Note, that distances are outgoing from the edge of the veins on both sides. Profile 5 was measured twice, once in the field with narrow spacing and once using the rock chips that were collected for conventional XRF. n.d. = not detected.

Appendix 2

*Analyses of the international reference materials AGV-2 (measured by conventional XRF) as well as NIST 612 and BCR-2G (measured by LA-ICP-MS)*

| type of analyses | conventional XRF | | | LA-ICP-MS | | | |
|---|---|---|---|---|---|---|---|
| international reference | AGV-2 | | | NIST 612 | | BCR-2G | |
| comment | average out of 10 analyses | expected | residual | average out of 20 analyses | standard deviation | average out of 3 analysis | standard deviation |
| in wt.% | | | | | | | |
| $SiO_2$ | 60.18 | 60.15 | 0.03 | | | | |
| $Al_2O_3$ | 17.09 | 17.15 | -0.06 | | | | |
| CaO | 5.23 | 5.27 | -0.04 | | | | |
| MgO | 1.78 | 1.82 | -0.04 | | | | |
| MnO | 0.10 | 0.10 | 0.00 | | | | |
| $P_2O_5$ | 0.67 | 0.49 | 0.19 | | | | |
| $Fe_2O_3$(tot) | 6.76 | 6.79 | -0.02 | | | | |
| $Na_2O$ | 4.23 | 4.25 | -0.02 | | | | |
| $K_2O$ | 2.91 | 2.92 | -0.01 | | | | |
| $TiO_2$ | 1.05 | 1.07 | -0.01 | | | | |
| in CPS (counts per second) | | | | | | | |
| Si | | | | 350850 | 109377 | 82333 | 5132 |
| in ppm | | | | | | | |
| Ca | | | | 98590 | 17726 | 75333 | 3055 |
| V | | | | 39.52 | 2.33 | 401.33 | 30.86 |
| Rb | | | | 32.08 | 2.40 | 43.17 | 3.07 |
| Sr | | | | 78.95 | 2.76 | 357.67 | 17.21 |
| Yb | | | | 38.18 | 1.49 | 32.07 | 2.22 |
| Zr | | | | 38.09 | 1.18 | 188.33 | 4.51 |
| Nb | | | | 40.11 | 1.65 | 13.70 | 0.26 |
| Cs | | | | 42.80 | 3.05 | 1.04 | 0.08 |
| Ba | | | | 40.12 | 2.28 | 716.67 | 20.82 |
| La | | | | 36.01 | 1.33 | 26.30 | 1.31 |
| Ce | | | | 39.15 | 2.42 | 55.10 | 1.85 |
| Pr | | | | 37.52 | 1.91 | 6.87 | 0.31 |
| Nd | | | | 36.12 | 1.63 | 29.77 | 2.03 |
| Sm | | | | 38.35 | 1.46 | 6.93 | 0.32 |
| Eu | | | | 35.08 | 0.92 | 2.06 | 0.02 |
| Gd | | | | 36.80 | 1.24 | 6.43 | 0.31 |
| Tb | | | | 36.20 | 1.37 | 0.96 | 0.03 |
| Dy | | | | 36.15 | 1.44 | 6.23 | 0.35 |
| Ho | | | | 38.05 | 1.20 | 1.30 | 0.06 |
| Er | | | | 38.13 | 0.80 | 3.65 | 0.03 |
| Tm | | | | 38.14 | 1.42 | 0.53 | 0.01 |
| Yb | | | | 39.28 | 1.33 | 3.62 | 0.16 |
| Lu | | | | 37.09 | 1.00 | 0.51 | 0.02 |
| Hf | | | | 35.25 | 1.54 | 4.89 | 0.19 |
| Ta | | | | 40.35 | 1.87 | 0.89 | 0.01 |
| Pb | | | | 39.62 | 3.92 | 9.63 | 0.25 |
| Th | | | | 38.08 | 1.70 | 6.60 | 0.10 |
| U | | | | 38.39 | 3.45 | 1.63 | 0.02 |

## REFERENCES

Abart, R., Badertscher, N., Burkhard, M., and Povoden, E., 2002, Oxygen, carbon and strontium isotope systematics in two profiles across the Glarus thrust: implications for fluid flow: Contributions to Mineralogy and Petrology, v. 143, n. 2, p. 192–208, http://dx.doi.org/10.1007/s00410-001-0326-5

Ague, J. J., 1994a, Mass transfer during Barrovian metamorphism of pelites, south-central Connecticut. I: Evidence for changes in composition and volume: American Journal of Science, v. 294, n. 8, p. 989–1057, http://dx.doi.org/10.2475/ajs.294.8.989

——— 1994b, Mass transfer during Barrovian metamorphism of pelites, south-central Connecticut. II: Channelized fluid flow and the growth of staurolite and kyanite: American Journal of Science, v. 294, n. 9, p. 1061–1134, http://dx.doi.org/10.2475/ajs.294.9.1061

——— 1997, Crustal mass transfer and index mineral growth in Barrow's garnet zone, northeast Scotland: Geology, v. 25, n. 1, p. 73–76, http://dx.doi.org/10.1130/0091-7613(1997)025<0073:CMTAIM>2.3.CO;2

——— 2003a, Fluid flow in the deep crust, *in* Rudnick, R., L., editor, The Crust: Treatise on Geochemistry, v. 3, p. 195–228, http://dx.doi.org/10.1016/B0-08-043751-6/03023-1

——— 2003b, Fluid infiltration and transport of major, minor, and trace elements during regional metamorphism of carbonate rocks, Wepawaug Schist, Connecticut, USA: American Journal of Science, v. 303, n. 9, p. 753–816, http://dx.doi.org/10.2475/ajs.303.9.753

——— 2007, Models of permeability contrasts in subduction zone mélange: Implications for gradients in fluid fluxes, Syros and Tinos Islands, Greece: Chemical Geology, v. 239, n. 3–4, p. 217–227, http://dx.doi.org/10.1016/j.chemgeo.2006.08.012

——— 2011, Extreme channelization of fluid and the problem of element mobility during Barrovian metamorphism: American Mineralogist, v. 96, n. 2–3, p. 333–352, http://dx.doi.org/10.2138/am.2011.3582

Ague, J. J., and van Haren, J. L. M., 1996, Assessing metasomatic mass and volume changes using the bootstrap, with application to deep crustal hydrothermal alteration of marble: Economic Geology, v. 91, n. 7, p. 1169–1182, http://dx.doi.org/10.2113/gsecongeo.91.7.1169

Altherr, R., Schliestedt, M., Okrusch, M., Seidel, E., Kreuzer, H., Harre, W., Lenz, H., Wendt, I., and Wagner, G. A., 1979, Geochronology of high-pressure rocks on Sifnos (Cyclades, Greece): Contributions to Mineralogy and Petrology, v. 70, n. 3, p. 245–255, http://dx.doi.org/10.1007/BF00375354

Aubouin, J., and Dercourt, J., 1965, Sur la géologie de l'Egée: regard sur la Crète (Grèce): Bulletin de la Société Géologique de France, v. 7, p. 787–821.

Austrheim, H., 1987, Eclogitization of lower crustal granulites by fluid migration through shear zones: Earth and Planetary Science Letters, v. 81, n. 2–3, p. 221–232, http://dx.doi.org/10.1016/0012-821X(87)90158-0

Avigad, D., 1993, Tectonic juxtaposition of blueschists and greenschists in Sifnos Island (Aegean Sea) - implications for the structure of the Cycladic blueschist belt: Journal of Structural Geology, v. 15, n. 12, p. 1459–1469, http://dx.doi.org/10.1016/0191-8141(93)90006-V

Avigad, D., Matthews, A., Evans, B. W., and Garfunkel, Z., 1992, Cooling during the exhumation of a blueschist terrane: Sifnos (Cyclades), Greece: European Journal of Mineralogy, v. 4, n. 3, p. 619–634, http://dx.doi.org/10.1127/ejm/4/3/0619

Barr, H., 1990, Preliminary fluid inclusion studies in a high-grade blueschist terrain, Syros, Greece: Mineralogical Magazine, v. 54, p. 159–168, http://dx.doi.org/10.1180/minmag.1990.054.375.03

Baumgartner, L. P., and Ferry, J. M., 1991, A model for coupled fluid-flow and mixed-volatile mineral reactions with applications to regional metamorphism: Contributions to Mineralogy and Petrology, v. 106, n. 3, p. 273–285, http://dx.doi.org/10.1007/BF00324557

Baumgartner, L. P., and Olsen, S. N., 1995, A least-squares approach to mass transport calculations using the isocon method: Economic Geology, v. 90, n. 5, p. 1261–1270, http://dx.doi.org/10.2113/gsecongeo.90.5.1261

Beinlich, A., Klemd, R., John, T., and Gao, J., 2010, Trace-element mobilization during Ca-metasomatism along a major fluid conduit: Eclogitization of blueschist as a consequence of fluid–rock interaction: Geochimica et Cosmochimica Acta, v. 74, n. 6, p. 1892–1922, http://dx.doi.org/10.1016/j.gca.2009.12.011

Bickle, M. J., 1992, Transport mechanisms by fluid-flow in metamorphic rocks: Oxygen and strontium decoupling in the Trois Seigneurs Massif– a consequence of kinetic dispersion?: American Journal of Science, v. 292, n. 5, p. 289–316, http://dx.doi.org/10.2475/ajs.292.5.289

Bickle, M. J., and Baker, J., 1990, Advective-diffusive transport of isotopic fronts: An example from Naxos, Greece: Earth and Planetary Science Letters, v. 97, n. 1–2, p. 78–93, http://dx.doi.org/10.1016/0012-821X(90)90100-C

Brady, J. B., 1988, The role of volatiles in the thermal history of metamorphic terranes: Journal of Petrology, v. 29, n. 6, p. 1187–1213, http://dx.doi.org/10.1093/petrology/29.6.1187

Breeding, C. M., and Ague, J. J., 2002, Slab-derived fluids and quartz-vein formation in an accretionary prism, Otago Schist, New Zealand: Geology, v. 30, n. 6, p. 499–502, http://dx.doi.org/10.1130/0091-7613(2002)030<0499:SDFAQV>2.0.CO;2

Breeding, C. M., Ague, J. J., Bröcker, M., and Bolton, E. W., 2003, Blueschist preservation in a retrograded, high-pressure, low-temperature metamorphic terrane, Tinos, Greece: Implications for fluid flow paths in subduction zones: Geochemistry, Geophysics, Geosystems, v. 4, n. 1, http://dx.doi.org/10.1029/2002GC000380

Breeding, C. M., Ague, J. J., and Bröcker, M., 2004, Fluid–metasedimentary rock interactions in subduction-zone mélange: Implications for the chemical composition of arc magmas: Geology, v. 32, n. 12, p. 1041–1044, http://dx.doi.org/10.1130/G20877.1

Bröcker, M., Kreuzer, H., Matthews, A., and Okrusch, M., 1993, $^{40}Ar/^{39}Ar$ and oxygen isotope studies of polymetamorphism from Tinos Island, Cycladic blueschist belt, Greece: Journal of Metamorphic Geology, v. 11, n. 2, p. 223–240, http://dx.doi.org/10.1111/j.1525-1314.1993.tb00144.x

Bröcker, M., Bieling, D., Hacker, B., and Gans, P., 2004, High-Si phengite records the time of greenschist

facies overprinting: Implications for models suggesting mega-detachments in the Aegean Sea: Journal of Metamorphic Geology, v. 22, n. 5, p. 427–442, http://dx.doi.org/10.1111/j.1525-1314.2004.00524.x
Camacho, A., Lee, J. K. W., Hensen, B. J., and Braun, J., 2005, Short-lived orogenic cycles and the eclogitization of cold crust by spasmodic hot fluids: Nature, v. 435, p. 1191–1196, http://dx.doi.org/10.1038/nature03643
Connolly, J. A. D., 1997, Devolatilization generated fluid pressure and deformation propagated fluid flow during prograde regional metamorphism: Journal of Geophysical Research: Solid Earth (1978–2012), v. 102, p. 18149–18173.
Connolly, J. A. D., and Thompson, A. B., 1989, Fluid and enthalpy production during regional metamorphism: Contributions to Mineralogy and Petrology, v. 102, n. 3, p. 347–366, http://dx.doi.org/10.1007/BF00373728
Dürr, S., Altherr, R., Keller, J., Okrusch, M., and Seidel, E., 1978, The median Aegean crystalline belt: stratigraphy, structure, metamorphism, magmatism, *in* Cloos, H., Roeder, H. C., and Schmidt, K., editors, Alps, Apennines, Hellenides: Inter-Union Commission on Geodynamics Scientific Report, v. 38, p. 455–476.
Evans, K. A., and Bickle, M. J., 1999, Determination of time-integrated metamorphic fluid fluxes from the reaction progress of multivariant assemblages: Contributions to Mineralogy and Petrology, v. 134, n. 2, p. 277–293, http://dx.doi.org/10.1007/s004100050484
Famin, V., Philippot, P., Jolivet, L., and Agard, P., 2004, Evolution of hydrothermal regime along a crustal shear zone, Tinos Island, Greece: Tectonics, v. 23, n. 5, TC5004, http://dx.doi.org/10.1029/2003TC001509
Ferry, J. M., 1983, Regional metamorphism of the Vassalboro Formation, south-central Maine, USA: a case study of the role of fluid in metamorphic petrogenesis: Journal of the Geological Society, v. 140, n. 5, p. 551–576, http://dx.doi.org/10.1144/gsjgs.140.4.0551
——— 1988, Contrasting mechanisms of fluid flow through adjacent stratigraphic units during regional metamorphism, south-central Maine, USA: Contributions to Mineralogy and Petrology, v. 98, n. 1, p. 1–12, http://dx.doi.org/10.1007/BF00371903
——— 1992, Regional metamorphism of the Waits River Formation, eastern Vermont: Delineation of a new type of giant metamorphic hydrothermal system: Journal of Petrology, v. 33, n. 1, p. 45–94, http://dx.doi.org/10.1093/petrology/33.1.45
Ferry, J. M., and Dipple, G. M., 1991, Fluid flow, mineral reactions, and metasomatism: Geology, v. 19, n. 3, p. 211–214, http://dx.doi.org/10.1130/0091-7613(1991)019<0211:FFMRAM>2.3.CO;2
Franz, G., and Liebscher, A., 2004, Physical and Chemical Properties of the Epidote Minerals–An Introduction–: Reviews in Mineralogy and Geochemistry, v. 56, n. 1, p. 1–81, http://dx.doi.org/10.2138/gsrmg.56.1.1
Ganor, J., Matthews, A., and Schliestedt, M., 1994, Post metamorphic low $\delta^{13}C$ calcite in the Cycladic complex (Greece) and their implications for modeling fluid infiltration processes using carbon isotope composition: European Journal of Mineralogy, v. 6, n. 3, p. 365–379, http://dx.doi.org/10.1127/ejm/6/3/0365
Ganor, J., Matthews, A., Schliestedt, M., and Garfunkel, Z., 1996, Oxygen isotopic heterogeneities of metamorphic rocks: an original tectonostratigraphic signature, or an imprint of exotic fluids? A case study of Sifnos and Tinos islands (Greece): European Journal of Mineralogy-Ohne Beihefte, v. 8, n. 4, p. 719–732, http://dx.doi.org/10.1127/ejm/8/4/0719
Hellstrom, J., Paton, C., Woodhead, J., and Hergt, J., 2008, Iolite: software for spatially resolved LA-(quad and MC) ICPMS analysis: Mineralogical Association of Canada Short Course Series, v. 40, p. 343–348.
Herms, P., John, T., Bakker, R. J., and Schenk, V., 2012, Evidence for channelized external fluid flow and element transfer in subducting slabs (Raspas Complex, Ecuador): Chemical Geology, v. 310–311, p. 79–96, http://dx.doi.org/10.1016/j.chemgeo.2012.03.023
Jacobshagen, V., Dürr, S., Kockel, F., Kopp, K. O., Kowalczyk, G., Berckhemer, H., and Büttner, D., 1978, Structure and geodynamic evolution of the Aegean region, *in* Cloos, H., Roeder, D., and Schmidt, K. E., editors, Alps, Apennines, Hellenides: Inter- Union Commission on Geodynamics Scientific Report, v. 38, p. 537–564.
Jiang, S.-Y., Wang, R.-C., Xu, X.-S., and Zhao, K.-D., 2005, Mobility of high field strength elements (HFSE) in magmatic-, metamorphic-, and submarine-hydrothermal systems: Physics and Chemistry of the Earth, Parts A/B/C, v. 30, n. 17–18, p. 1020–1029, http://dx.doi.org/10.1016/j.pce.2004.11.004
Jochum, K. P., Weis, U., Stoll, B., Kuzmin, D., Yang, Q., Raczek, I., Jacob, D. E., Stracke, A., Birbaum, K., Frick, D. A., Günther, D., and Ensweiler, J., 2011, Determination of reference values for NIST SRM 610–617 glasses following ISO guidelines: Geostandards and Geoanalytical Research, v. 35, n. 4, p. 397–429, http://dx.doi.org/10.1111/j.1751-908X.2011.00120.x
John, T., Gussone, N., Podladchikov, Y. Y., Bebout, G. E., Dohmen, R., Halama, R., Klemd, R., Magna, T., and Seitz, H.-M., 2012, Volcanic arcs fed by rapid pulsed fluid flow through subducting slabs: Nature Geoscience, v. 5, p. 489–492, http://dx.doi.org/10.1038/ngeo1482
Jolivet, L., and Brun, J.-P., 2010, Cenozoic geodynamic evolution of the Aegean: International Journal of Earth Sciences, v. 99, n. 1, p. 109–138, http://dx.doi.org/10.1007/s00531-008-0366-4
Keiter, M., Ballhaus, C., and Tomaschek, F., 2011, A new geological map of the Island of Syros (Aegean Sea, Greece): Implications for lithostratigraphy and structural history of the Cycladic Blueschist Unit: Geological Society of America Special Papers, v. 481, p. 1–43, http://dx.doi.org/10.1130/2011.2481
Kleine, B. I., Skelton, A. D. L., Huet, B., and Pitcairn, I. K., 2014, Preservation of Blueschist-facies Minerals along a Shear Zone by Coupled Metasomatism and Fast-flowing $CO_2$-bearing Fluids: Journal of Petrology, v. 55, n. 10, p. 1905–1939, http://dx.doi.org/10.1093/petrology/egu045
Lagos, M., Scherer, E. E., Tomaschek, F., Münker, C., Keiter, M., Berndt, J., and Ballhaus, C., 2007, High

precision Lu-Hf geochronology of Eocene eclogite-facies rocks from Syros, Cyclades, Greece: Chemical Geology, v. 243, n. 1–2, p. 16–35, http://dx.doi.org/10.1016/j.chemgeo.2007.04.008

Léger, A., and Ferry, J. M., 1993, Fluid infiltration and regional metamorphism of the Waits River Formation, North-east Vermont, USA: Journal of Metamorphic Geology, v. 11, n. 1, p. 3–29, http://dx.doi.org/10.1111/j.1525-1314.1993.tb00128.x

Liebscher, A., Thiele, M., Franz, G., Dörsam, G., and Gottschalk, M., 2009, Synthetic Sr-Ca margarite, anorthite and slawsonite solid solutions and solid-fluid Sr-Ca fractionation: European Journal of Mineralogy, v. 21, n. 2, p. 275–292, http://dx.doi.org/10.1127/0935-1221/2009/0021-1917

Maluski, H., Bonneau, M., and Kienast, J. R., 1987, Dating the metamorphic events in the Cycladic area; $^{39}Ar/^{40}Ar$ data from metamorphic rocks of the island of Syros (Greece): Bulletin de la Société géologique de France, v. 3, n. 5, p. 833–842, http://dx.doi.org/10.2113/gssgfbull.III.5.833

Marschall, H. R., Ludwig, T., Altherr, R., Kalt, A., and Tonarini, S., 2006, Syros metasomatic tourmaline: Evidence for very high-$\delta^{11}B$ fluids in subduction zones: Journal of Petrology, v. 47, n. 10, p. 1915–1942, http://dx.doi.org/10.1093/petrology/egl031

McCaig, A. M., Wayne, D. M., Marshall, J. D., Banks, D., and Henderson, I., 1995, Isotopic and fluid inclusion studies of fluid movement along the Gavarnie Thrust, central Pyrenees: Reaction fronts in carbonate mylonites: American Journal of Science, v. 295, n. 3, p. 309–343, http://dx.doi.org/10.2475/ajs.295.3.309

Miller, D. P., Marschall, H. R., and Schumacher, J. C., 2009, Metasomatic formation and petrology of blueschist-facies hybrid rocks from Syros (Greece): Implications for reactions at the slab–mantle interface: Lithos, v. 107, n. 1–2, p. 53–67, http://dx.doi.org/10.1016/j.lithos.2008.07.015

Morimoto, N., 1988, Nomenclature of pyroxenes: Mineralogy and Petrology, v. 39, n. 1, p. 55–76, http://dx.doi.org/10.1007/BF01226262

Neretnieks, I., Eriksen, T., and Tähtinen, P., 1982, Tracer movement in a single fissure in granitic rock: Some experimental results and their interpretation: Water Resources Research, v. 18, n. 4, p. 849–858, http://dx.doi.org/10.1029/WR018i004p00849

Norton, D., and Knapp, R., 1977, Transport phenomena in hydrothermal systems: The nature of porosity: American Journal of Science, v. 277, n. 8, p. 913–936, http://dx.doi.org/10.2475/ajs.277.8.913

Okrusch, M., and Bröcker, M., 1990, Eclogites associated with high-grade blueschists in the Cyclades archipelago, Greece: A review: European Journal of Mineralogy, v. 2, p. 451–478.

Parra, T., Vidal, O., and Jolivet, L., 2002, Relation between the intensity of deformation and retrogression in blueschist metapelites of Tinos Island (Greece) evidenced by chlorite-mica local equilibria: Lithos, v. 63, n. 1–2, p. 41–66, http://dx.doi.org/10.1016/S0024-4937(02)00115-9

Paton, C., Hellstrom, J., Paul, B., Woodhead, J., and Hergt, J., 2011, Iolite: Freeware for the visualisation and processing of mass spectrometric data: Journal of Analytical Atomic Spectrometry, v. 26, p. 2508–2518, http://dx.doi.org/10.1039/c1ja10172b

Peacock, S. M., 1989, Numerical constraints on rates of metamorphism, fluid production, and fluid flux during regional metamorphism: Geological Society of America Bulletin, v. 101, n. 4, p. 476–485, http://dx.doi.org/10.1130/0016-7606(1989)101<0476:NCOROM>2.3.CO;2

Penniston-Dorland, S. C., and Ferry, J. M., 2008, Element mobility and scale of mass transport in the formation of quartz veins during regional metamorphism of the Waits River Formation, east-central Vermont: American Mineralogist, v. 93, n. 1, p. 7–21, http://dx.doi.org/10.2138/am.2008.2461

Penniston-Dorland, S. C., Sorensen, S. S., Ash, R. D., and Khadke, S. V., 2010, Lithium isotopes as a tracer of fluids in a subduction zone mélange: Franciscan Complex, CA: Earth and Planetary Science Letters, p. 292, n. 1–2, p. 181–190, http://dx.doi.org/10.1016/j.epsl.2010.01.034

Pogge von Strandmann, P. A. E., Dohmen, R., Marschall, H. R., Schumacher, J. C., and Elliott, T., 2015, Extreme magnesium isotope fractionation at outcrop scale records the mechanism and rate at which reaction fronts advance: Journal of Petrology, v. 56, n. 1, p. 33–58, http://dx.doi.org/10.1093/petrology/egu070

Putlitz, B., Matthews, A., and Valley, J. W., 2000, Oxygen and hydrogen isotope study of high-pressure metagabbros and metabasalts (Cyclades, Greece): implications for the subduction of oceanic crust: Contributions to Mineralogy and Petrology, v. 138, n. 2, p. 114–126, http://dx.doi.org/10.1007/s004100050012

Putlitz, B., Cosca, M. A., and Schumacher, J. C., 2005, Prograde mica $^{40}Ar/^{39}Ar$ growth ages recorded in high pressure rocks (Syros, Cyclades, Greece): Chemical Geology, v. 214, n. 1–2, p. 79–98, http://dx.doi.org/10.1016/j.chemgeo.2004.08.056

Putnis, A., and Austrheim, H., 2010, Fluid-induced processes: metasomatism and metamorphism: Geofluids, v. 10, n. 1–2, p. 254–269, http://dx.doi.org/10.1111/j.1468-8123.2010.00285.x

Schliestedt, M., and Matthews, A., 1987, Transformation of blueschist to greenschist facies rocks as a consequence of fluid infiltration, Sifnos (Cyclades), Greece: Contributions to Mineralogy and Petrology, v. 97, n. 2, p. 237–250, http://dx.doi.org/10.1007/BF00371243

Schumacher, J. C., Brady, J. B., and Cheney, J. T., 2008a, Metamorphic style and development of the blueschist-to eclogite-facies rocks, Cyclades, Greece, IOP Conference Series: IOP Conference Series, Earth and Environmental Science, v. 2, n. 1, p. 012017, http://dx.doi.org/10.1088/1755-1307/2/1/012017

Schumacher, J. C., Brady, J. B., Cheney, J. T., and Tonnsen, R. R., 2008b, Glaucophane-bearing marbles on Syros, Greece: Journal of Petrology, v. 49, n. 9, p. 1667–1686, http://dx.doi.org/10.1093/petrology/egn042

Shaw, D. M., 1954, Trace elements in pelitic rocks Part I: Variation during metamorphism: Geological Society of America Bulletin, v. 65, n. 12, p. 1151–1166, http://dx.doi.org/10.1130/0016-7606(1954)65[1151:TEIPR]2.0.CO;2

——— 1956, Geochemistry of pelitic rocks. Part III: Major elements and general geochemistry: Geological

Society of America Bulletin, v. 67, n. 7, p. 919–934, http://dx.doi.org/10.1130/0016-7606(1956)67[919:GOPRPI]2.0.CO;2
Skelton, A., 2011, Flux rates for water and carbon during greenschist facies metamorphism: Geology, v. 39, n. 1, p. 43–46, http://dx.doi.org/10.1130/G31328.1
Skelton, A. D. L., Graham, C. M., and Bickle, M. J., 1995, Lithological and structural controls on regional 3-D fluid flow patterns during greenschist facies metamorphism of the Dalradian of the SW Scottish Highlands: Journal of Petrology, v. 36, n. 2, p. 563–586, http://dx.doi.org/10.1093/petrology/36.2.563
Tanner, P. W. G., and Miller, R. G., 1980, Geochemical evidence for loss of Na and K from Moinian calc-silicate pods during prograde metamorphism: Geological Magazine, v. 117, n. 3, p. 267–275, http://dx.doi.org/10.1017/S001675680003048X
Tomaschek, F., Kennedy, A. K., Villa, I. M., Lagos, M., and Ballhaus, C., 2003, Zircons from Syros, Cyclades, Greece - Recrystallization and Mobilization of Zircon During High-Pressure Metamorphism: Journal of Petrology, v. 44, n. 11, p. 1977–2002, http://dx.doi.org/10.1093/petrology/egg067
Trotet, F., Jolivet, L., and Vidal, O., 2001a, Tectono-metamorphic evolution of Syros and Sifnos islands (Cyclades, Greece): Tectonophysics, v. 338, n. 2, p. 179–206, http://dx.doi.org/10.1016/S0040-1951(01)00138-X
Trotet, F., Vidal, O., and Jolivet, L., 2001b, Exhumation of Syros and Sifnos metamorphic rocks (Cyclades, Greece). New constraints on the PT paths: European Journal of Mineralogy, v. 13, n. 5, p. 901–902, http://dx.doi.org/10.1127/0935-1221/2001/0013/0901
Van der Plas, L., and Tobi, A. C., 1965, A chart for judging the reliability of point counting results: American Journal of Science, v. 263, n. 1, p. 87–90, http://dx.doi.org/10.2475/ajs.263.1.87
Walther, J. V., and Orville, P. M., 1982, Volatile production and transport in regional metamorphism: Contributions to Mineralogy and Petrology, v. 79, n. 3, p. 252–257, http://dx.doi.org/10.1007/BF00371516
Walther, J. V., and Wood, B. J., 1984, Rate and mechanism in prograde metamorphism: Contributions to Mineralogy and Petrology, v. 88, n. 3, p. 246–259, http://dx.doi.org/10.1007/BF00380169
Wark, D. A., and Watson, E. B., 2004, Interdiffusion of $H_2O$ and $CO_2$ in metamorphic fluids at ~ 490 to 690 °C and 1 GPa: Geochimica et Cosmochimica Acta, v. 68, n. 12, p. 2693–2698, http://dx.doi.org/10.1016/j.gca.2003.12.006
Wijbrans, J. R., Schliestedt, M., and York, D., 1990, Single grain argon laser probe dating of phengites from the blueschist to greenschist transition on Sifnos (Cyclades, Greece): Contributions to Mineralogy and Petrology, v. 104, n. 5, p. 582–593, http://dx.doi.org/10.1007/BF00306666
Wood, B. J., and Walther, J. V., 1983, Rates of hydrothermal reactions: Science, v. 222, p. 413–415, http://dx.doi.org/10.1126/science.222.4622.413
Zhao, Z., and Skelton, A., 2013, Simultaneous calculation of metamorphic fluid fluxes, reaction rates and fluid–rock interaction timescales using a novel inverse modeling framework: Earth and Planetary Science Letters, v. 373, p. 217–227, http://dx.doi.org/10.1016/j.epsl.2013.05.007